4-2013

Adsorption of Hexavalent Chromium On Hydrous Manganese Oxide

Andrew K. MacLeod
Western Michigan University

ADSORPTION OF HEXAVALENT CHROMIUM ON HYDROUS MANGANESE OXIDE

by

Andrew MacLeod

A thesis submitted to the Graduate College
in partial fulfillment of the requirements
for the degree of Master of Science
Geosciences
Western Michigan University
April 2013

Thesis Committee:

Dr. Carla Koretsky, Ph.D., Chair
Dr. Duane Hampton, Ph.D.
Dr. R.V. Krishnamurthy, Ph.D.

ADSORPTION OF HEXAVALENT CHROMIUM ONTO HYDROUS MANGANESE OXIDE

Andrew MacLeod, M.S.

Western Michigan University, 2013

Hexavalent chromium is a very common contaminant most often associated with industrial processes, it is quite mobile in the subsurface and a better understanding of its mobility and interactions with soil constituents will help ongoing remediation efforts.

Hydrous manganese oxides (HMO) are a very common soil constituent and thus would be likely to interact with Cr(VI) in contaminated shallow subsurface environments. The goal of this study is to develop a working model that can improve predictions of Cr(VI) mobility in natural systems. A diffuse double layer surface complexation model (DLM) was developed by deriving reaction stoichiometries and stability constants for formation of Cr(VI) surface complexes on HMO. These reaction stoichiometries and their respective stability constants were derived based on a DLM already developed by Tonkin et al. (2004) to describe the surface charging behavior of HMO.

To derive the Cr adsorption reaction stoichiometries and their respective stability constants, adsorption edge experiments were conducted under varying pH (~3-10) and ionic strength (0.001 to 0.1 M $NaNO_3$) under 0% pCO_2 conditions on synthetic hydrous manganese oxide. These adsorption edge data were used to constrain the Cr surface reactions in the absence of carbonate using the optimization program FITEQL. To account for carbonate interactions in natural systems, reaction stoichiometries and stability constants for competing carbonate surface complexes were derived using experimental data collected under varying pH and ionic strength at 5% pCO_2. The DLM was tested against experimental data collected at atmospheric and 2.5% pCO2 under a wide range of pH and ionic strength conditions.

ACKNOWLEDGMENTS

I would like to first whole-heartedly acknowledge and thank Dr. Carla Koretsky for taking me in as an undergraduate student many years ago. She gave me opportunities I never dreamed possible and I wouldn't be where I am today if it weren't for her. I would also like to thank my committee members Dr. Krishnamurthy and Dr. Hampton for taking the time to help me with my project, to read my whole thesis and to provide me with the support and feed back they did. I would also like to thank my lab colleagues Michelle Barger, Ryan Sibert, Anne Gilchrist, and Thomas Reich for helping to form my laboratory skills, work ethic, and teaching me if something is broke, taking it apart into teeny tiny pieces isn't going to break it more. I would like to thank my beautiful and incredibly supportive wife Anne Marie Olbrot for believing in me, supporting me and of course feeding me better than anyone I know. Without her this would not have been possible. I also would like to acknowledge my parents for all of their love and support, my ping pong think break partners, Kathy Wright for making my graduation even a possibility, and of course Bell's Brewery for everything.

Andrew K. MacLeod

TABLE OF CONTENTS

Table of Contents—continued

LIST OF TABLES

LIST OF FIGURES

CHAPTER I

INTRODUCTION

Background

Hexavalent chromium, Cr(VI), has many industrial uses including wood preservation, leather tanning, paint pigments, and electroplating (Huang and Wu, 1975; Barnhart, 1997; ATSDR, 2012). The United States imports the majority of its chromium from South Africa and Kazakhstan, importing 210 tons in 2007 alone (ATSDR, 2012). Cr(VI), however, is a known carcinogen that can cause lung cancer when inhaled and has been shown to increase the chance of stomach tumors when ingested by animals in laboratory testing (Grevatt, 1998; ATSDR, 2012). Cr(VI) is also toxic when ingested (Cohen et al., 1993; Costa, 1997; Costa and Klein, 2006; Holmes et al., 2008; Grevatt, 1998) and is known to cause kidney, liver, or blood cell damage, and even death (WHO, 1996; Grevatt, 1998). Cr(VI) contamination is fairly commonplace in the United States, and the Environmental Protection Agency has identified Cr(VI) contamination in over half of the National Priority List hazardous waste sites (ASTDR, 2012).

Chromium Geochemistry

In contaminated shallow aquifers where oxic conditions persist, Cr(VI) typically exists as bichromate ($HCrO_4^-$) and chromate (CrO_4^{2-}) anions and is very mobile as a dissolved species (Barnhart, 1997; Grevatt, 1998; U.S. EPA, 1999). Under suboxic or anoxic conditions, however, Cr(VI) may be reduced to the less mobile Cr(III) by redox reactions with iron-sulfide minerals (Patterson et al., 1997; U.S. EPA, 1999) or organic matter (Jardine et al. 1999; Daneshvar, 2002; Grevatt, 1998 U.S. 1999). The mobility of Cr(VI) may also be hampered by adsorption onto

solid surfaces from the aqueous solution (Huang and Wu, 1975; U.S. EPA, 1999). Understanding the causes and degree to which Cr(VI) will sorb to soil and sediment particulates is critical in understanding movement of Cr(VI) in the subsurface. Understanding this movement will lead to better remediation of contaminated soils and groundwaters by adding much greater predictive power to contaminant models focusing on Cr(VI).

Manganese and Hydrous Manganese Oxide Geochemistry

Manganese is the 10th most abundant element, comprising 0.1% of the Earth's crust (Post, 1999). In natural systems, it is a major constituent of minerals, including birnessite, braunite, pyrolusite, manganite and cryptomelane (Nesse, 2001). Many of these manganese-bearing minerals, such as birnessite and pyrolusite, are commonly found in soils (Post, 1999). A general name for these particular mineral oxides is hydrous manganese oxide (HMO). Chromium is often associated with Mn in soils; Mn^{4+} can oxidize Cr(III) to the more mobile Cr(VI) and become reduced to Mn^{2+} in suboxic and anoxic environments (Eary and Ral, 1987; Fendorf and Zasoski, 1992; Tokunga et al., 2007; Dai et al., 2009; Borch et al., 2010).

The synthetic manganese oxide used for this study is δ-MnO_2, an amorphous precursor to birnessite, furthermore referred to simply as HMO. It is synthesized in the laboratory, as a pure commercial supply is currently cost prohibitive. As HMO is an important constituent of soils, it has strong potential to affect the mobility of Cr(VI) due to its abundance in natural systems and the aforementioned association and reactions with chromium (Davison, 1993; Balistrieri et al., 1992b).

Adsorption and Surface Complexation Models (SCMs)

Adsorption is the interaction of aqueous chemical species through electrostatic and chemical interactions with the surface of a mineral. The larger the surface area of the mineral, all else being equal, the greater the potential for more sorbate to bind to the surface. These interactions are a result of electrical and chemical gradients within

the solution, including influences from solution pH, ionic strength and mineral surface charges. Bonds at the mineral surface may be coordinatively unsaturated, contributing to chemical interactions with aqueous species (Figure 1.1). Chemical gradients in, for example, solution ionic strength and pH, may also encourage or discourage chemical reactions at the mineral surface.

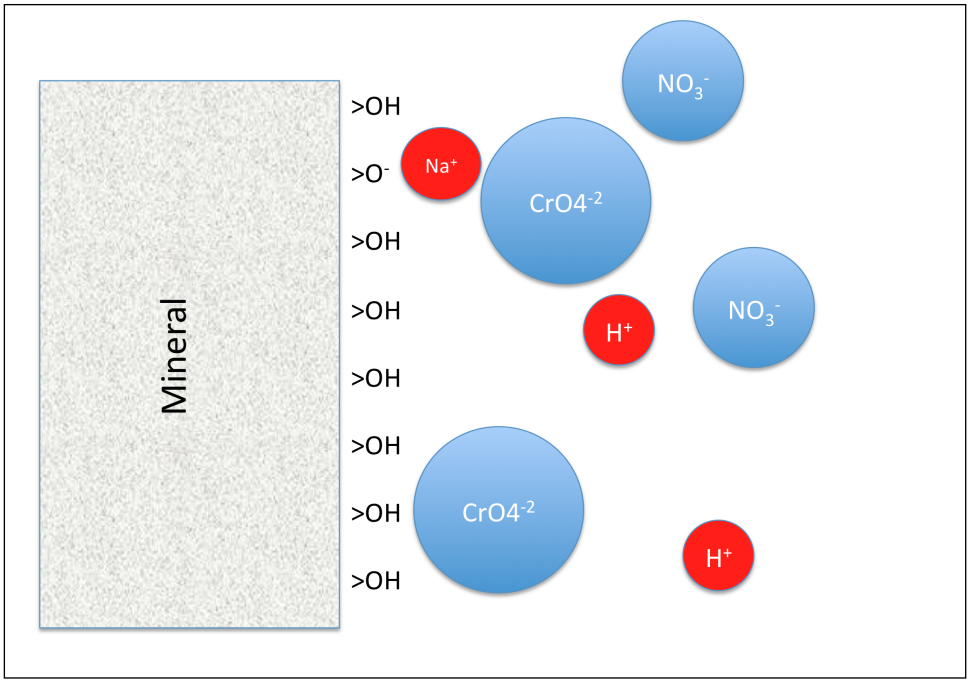

Figure 1.1 Mineral surface with sorbed chromate ions adsorbed on the surface.

The mineral surface may exhibit a net electrostatic charge for several reasons. First, there can be charge imbalance due to substitution of ions of different charge within the crystal lattice, leading to formation of a "permanent" or "structural" charge; this is most commonly observed in clay minerals. Charge can also arise due to coordinately unsaturated atoms at the solid surface, which may protonate or deprotonate, to produce net positive or negative charge, depending on the mineral chemistry and the solution pH. The resulting electrical double layer on the mineral surface can attract or repel aqueous ions. This may result in competitive interactions

between numerous aqueous species that could interact with the mineral surface (Eby, 2004).

Surface complexation models (SCMs), which were first developed in the 1960's, are used to represent interactions between a solid surface and aqueous chemical species (Dzombak and Morel, 1990). These interactions are affected by many parameters including pH, ionic strength of the aqueous solution, concentration of the sorbate, pCO_2, and the presence of organics or other ions in solution. These factors can either increase the adsorption of the aqueous species to the mineral surface or may impede the adsorption.

All SCMs have four major stipulations in common. First, the models assume that mineral surfaces are flat planes with one or more surface sites that can either protonate to yield a positive charge or deprotonate to yield a negative charge. Second, reactions at the mineral surface are assumed to be in local equilibrium and are described using mass law equations. Third, all SCMs are assumed to have variable surface charge directly resulting from chemical reactions at the surface. These are based on the particular pH that corresponds to the pristine point of zero charge (PPZC), the pH at which the mineral surface theoretically has an overall electric neutrality. Lastly, all SCMs are based on measured equilibrium constants that can be used to derive intrinsic equilibrium constants through the use of Coulombic correction factors (Koretsky, 2000).

The diffuse layer model (DLM) is an SCM that utilizes the Gouy-Chapman theory to describe the charged surface/water interface. This interface is comprised of two layers of charge, the charge of the surface that extends out into the surrounding solution, and the oppositely charged ions that are attracted to this charge (Dzombak and Morel, 1990). The extent, or size of the electrical double layer (edl) is largely determined by the solution ionic strength. With greater ionic strength, the influence of the edl contracts, and with lower ionic strength the edl influence expands away from the surface. The size of the diffuse layer can directly affect ion adsorption, depending on the charges of both the sorbate and the mineral surface. For example, if the sorbate

and the mineral surface are similarly charged, the sorbate will be strongly attracted to the oppositely charged edl and subsequently more sorbate will be adsorbed. However, if the sorbate and edl have the same charge, then a larger edl will repel like-charged ions, yielding less adsorption than a more contracted edl.

Previously Published HMO Surface Complexation Models

Several authors have conducted numerous experimental efforts to determine surface area, pH_{PPZC}, and site densites for HMO. These parameters were compiled by Tonkin et al. (2004) and utilized to develop SCM model parameters (Table 1.1).

Table 1.1 Model parameters utilized by Tonkin et al. (2004).

Author	Ionic strengths	Specific Surface area	Site Density (method)	PPZC
McKenzie (1981)	0.001 M $NaNO_3$ 0.01 M $NaNO_3$ 0.1 M $NaNO_3$ 0.5 M $NaNO_3$	105 m^2g^{-1} BET-N_2	22 µmol m^{-2} (alkalimetric titration)	3.0
Balistrieri and Murray (1982)	0.1 M NaCL 1 M NaCl	74 m^2g^{-1} BET-N_2	367 µmol m^{-2} (tritium exchange)	1.5 ±0.2
Catts and Langmuir (1986)	0.001 M $NaNO_3$ 0.01 M $NaNO_3$ 0.1 M $NaNO_3$	290 m^2g^{-1} BET-N_2	30 µmol m^{-2} (tritium exchange)	2.3 ±0.2
Fu et al. (1991)	0.001 M $NaNO_3$ 0.01 M $NaNO_3$ 0.1 M $NaNO_3$	296 m^2g^{-1} BET-N_2	13.6 µmol m^{-2} (alkalimetric titration)	NA
Ran and Fu (1999)	0.001 M $NaNO_3$ 0.1 M $NaNO_3$ 0.5 M $NaNO_3$	93 m^2g^{-1} BET-N_2	28.1 µmol m^{-2} (alkalimetric titration)	1.48
Pretorius and Linder (2001)	0.1 M KNO_3	331 m^2g^{-1} BET-N_2	8.8 µmol m^{-2} (alkalimetric titration)	NA
Davis and Kent (1991)	NA	NA	3.84 µmol m^{-2} (recommended for all mineral surfaces)	NA
Drits et. al. (1997)	NA	746 m^2g^{-1} theoretical value	2.8 µmol m^{-2} theoretical value	NA

The specific surface area (SSA) values compiled by Tonkin et al. (2004) were all measured using BET-N_2, except the value from Drits et al. (1997), which was derived theoretically using unit cell measurements for Na-birnessite structures in conjunction with the formula weight of MnO_2 to derive the surface area of 746 m^2 g^{-1}. The

measured values reported in Table 1.1, however, are significantly less than the theoretically derived value of 746 m^2 g^{-1} (Drits et al. 1997) that was used by Tonkin et al. (2004). Tonkin et al. (2004) attribute this discrepancy to experimental error, effects from aging and drying, and natural inherent differences in mineral surfaces. The difference between the theoretical and measured values has also been attributed to improper measurement of microporosity by BET-N_2, as the N_2 molecules may be too large to fit between layers that are readily accessible to smaller molecules and elements, such as protons and many other sorbates (Dzombak and Morel, 1990).

Site densities are difficult to measure directly. For this reason, site densities are sometimes calculated mathematically by considering the crystallography of the sorbent. Tonkin et al. (2004) used the site densities for HMO derived by Drits et al. (1997) using XRD measurements of Na-birnessite to obtain a detailed description of the Mn cation distribution and the structure of interlayer cations (ranging from $Na_{0.33}$, $Mn^{4+}_{0.67}$, $Mn^{3+}_{0.33}$ to $Na_{0.167}$, $Mn^{4+}_{0.833}$, $Mn^{3+}_{0.167}$ (Drits et. al., 1997)). They used these stoichiometries to determine the number of surface cations per layer octahedron, or moles of surface sites per mole of Mn. Site densities of 1.40-2.80 mmol g^{-1} HMO were calculated using the formula weight of 119 g mol^{-1} (Giovanoli et al., 1970) and the average of these site densities, 2.10 mmol g^{-1}, was used by Tonkin et al. (2004). Once Tonkin et al. (2004) had calculated the total site density, they divided the total site density into two fractions to represent the concentration of both the more abundant >XOH and less abundant >YOH surface sites. The relative site densities were derived using best-fits of potentiometric titration data.

Acid dissociation constants for each of the two surface site types were determined by Tonkin et al. (2004) using seven previously published titration data sets (Murray, 1974; McKenzie, 1981; Balistieri and Murray, 1982; Catts and Langmuir, 1986; Fu et al., 1991; Ran and Fu, 1999; Pretorius and Linder, 2001). These data sets where chosen because they used HMO similar to naturally occurring HMO. All the studies shown in Table 1.1 report a pH_{PPZC} of 3 or less, indicating the surface will maintain a net neutral or negative surface charge within the typical

operating pH range (~3-10). For this reason, Tonkin et al. (2004) only derive stability constants for the deprotonation reactions:

$$>SOH = >SO^- + H^+ \quad (1.1)$$

where "S" indicates with a unique site represented as either an X or a Y. They do not include stability constants for protonation in their model.

Tonkin et al. (2004) also derived stability constants for adsorption of a wide range of cations on HMO (Ba^{2+}, Ca^{2+}, Cd^{2+}, Co^{2+}, Cu^{2+}, Mg^{2+}, Mn^{2+}, Ni^{2+}, Pb^{2+}, Sr^{2+}, and Zn^{2+}) using previously published experimental data. However, they did not derive stability constants for chromium or other anion adsorption. Therefore, the DLM published by Tonkin et al. (2004) was expanded in this study to include chromium adsorption stability constants derived with FITEQL using experimental data collected in this study. Because the thermodynamic database program Visual MINTEQ (Allison et al., 1991) already includes the Tonkin et al. (2004) DLM, it is straightforward to add additional constants to describe chromate adsorption.

Objective

The main objective of this study is to derive reaction stoichiometries and equilibrium constants to describe Cr(VI) adsorption on HMO over a wide range of solution conditions. Specifically, laboratory experiments are used to derive Cr(VI) diffuse double layer surface complexation model stability constants. Variable experimental conditions used to constrain these constants are: pH (~3-10), ionic strength (0.001 to 0.1 M $NaNO_3$), pCO_2 (0-5%) and surface loadings (20 g/L HMO with $1 \cdot 10^{-5}$ - $2 \cdot 10^{-5}$ M Cr(VI)).

CHAPTER II

METHODS

HMO Synthesis

Hydrous manganese oxide (HMO) was synthesized using alkametric titration, according to the method of Stroes-Gascoyne et al. (1987). Under 0% pCO_2 conditions in a Coy glove box (95% N_2/5% H_2 atmosphere), a 900 mL solution containing 5.6 g $Mn(NO_3)_2 \cdot 4H_2O$ was stirred while a 100 mL solution containing 2.2 g $KMnO_4$ and 1.6 g KOH was added by fast drop-wise addition. The solution was stirred for 1 hour, and was then poured into six 50 mL centrifuge tubes. Each tube was centrifuged for 7 min at 6000 rpm in an Eppendorf centrifuge 5810. The supernatant was then poured off and more HMO solution was added to the tubes, which were shaken to resuspend the HMO from the bottom of the tubes. This was repeated until all 1000 mL of the HMO solution was condensed into the six 50 mL tubes. The HMO was then rinsed by adding ultrapure (>18 MΩ) water (DDI) to the tubes. The tubes were shaken to suspend the solids and to ensure the solid was in contact with the DDI water, and then the tubes were centrifuged and the supernatant poured off. This was repeated until the supernatant conductivity was less than that of a 0.001 M solution of $NaNO_3$. The tubes were then placed in an anaerobic hermetically sealed freezer bag, frozen for at least 24 hours, freeze-dried and subsequently stored under anaerobic conditions. The HMO product was verified through measurements of X-ray diffraction (XRD) patterns (Figure 2.1), and 11-pt N_2 BET surface area (specific surface area ~230 m^2g^{-1} with a range from 226 m^2g^{-1} to 317 m^2g^{-1}) that was compared to and comparable to published surface areas for HMO.

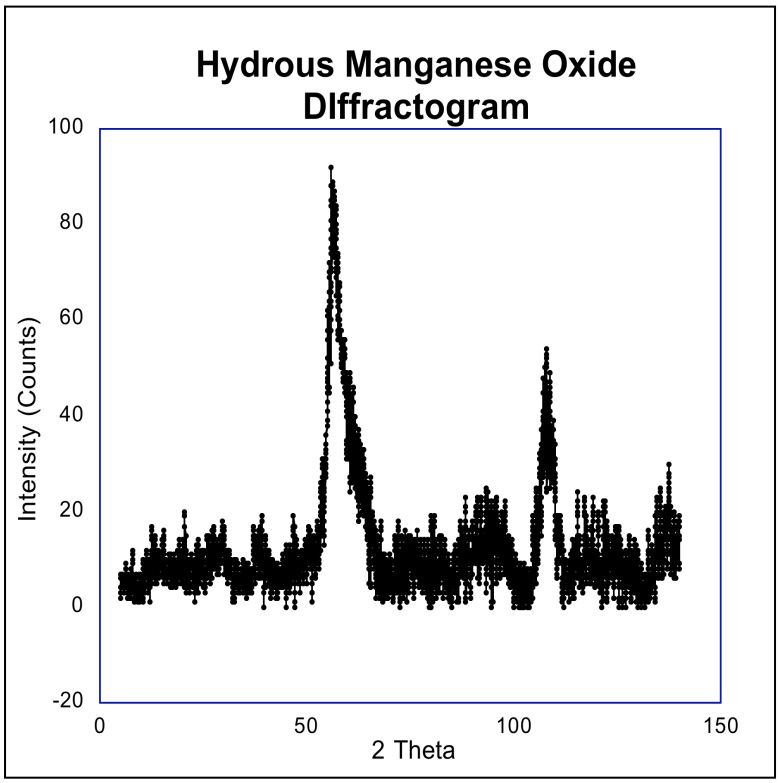

Figure 2.1 X-ray diffractogram of synthesized HMO measured with Cr-K alpha radiation.

Kinetic Investigations

Two initial kinetic experiments were conducted to determine adsorption reversibility as well as the length of time required for Cr(VI) adsorption on HMO to reach equilibrium. These experiments were conducted as follows: a 250 mL batch solution of $1 \cdot 10^{-5}$ M Cr(VI) and 0.001 M $NaNO_3$ was created and a 10 mL control aliquot was removed. Next, HMO was added to the remaining batch solution, at a concentration of 5 g/L and 10 g/L, for the first and second experiment, respectively. The resulting slurry was immediately titrated down to a pH of 3 by addition of trace-metal grade nitric acid and timing of the adsorption reaction(s) began. An initial 10 mL aliquot of the slurry was removed, while the pH was close to 3. Additional aliquots were removed at increasingly large time intervals over a total of 19.42 and 43.95 hours for the first and second experiments, respectively. After removal, each

aliquot of slurry was immediately centrifuged for approximately 5 minutes, and then filtered (0.2 µm syringe-filter). The pH of the remaining batch slurry was then raised by titration with concentrated trace metal grade NaOH to a pH of ~10 to determine the reversibility of Cr(VI) adsorption. The first experiment showed 97% of the adsorbed Cr(VI) desorbed after 29 min at pH ~10, and the second experiment showed 93% of the adsorbed Cr(VI) desorbed 83 min after the pH was raised to ~10. Within the first 5-10 min, ~90% of the Cr(VI) desorbed, thus indicating rapid and complete reversibility of adsorption (Figure 2.2).

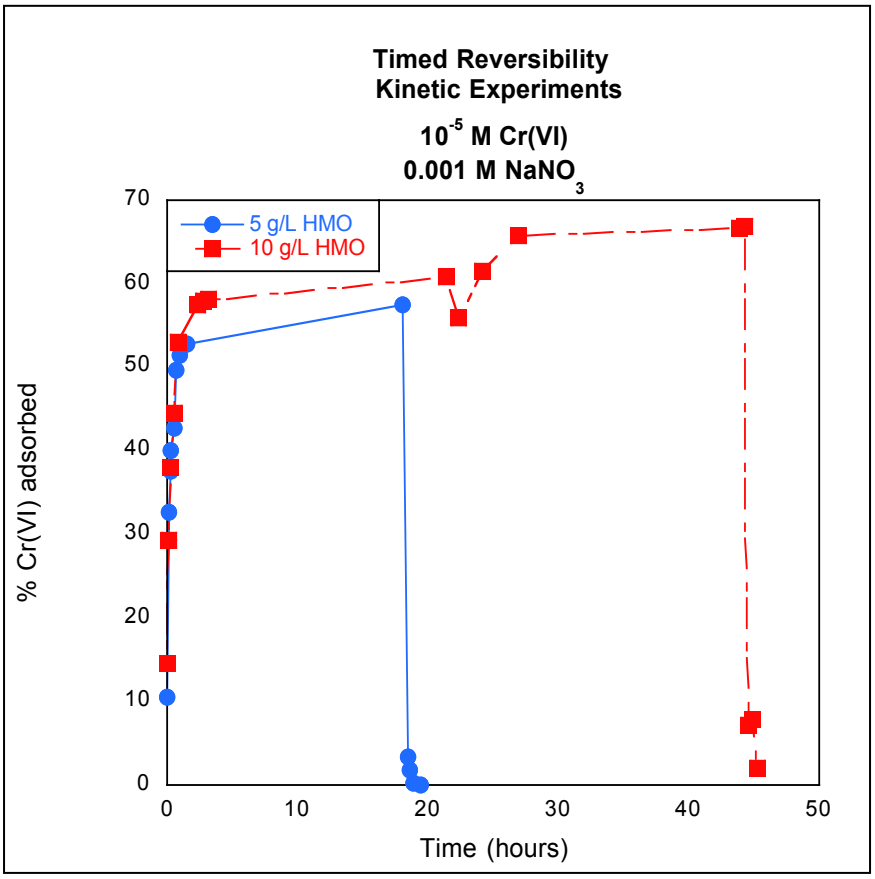

Figure 2.2 Cr(VI) adsorption and desorption kinetics, $1 \cdot 10^{-5}$ M Cr(VI) and 5 and 10 g/L HMO.

In addition to these experiments, initial pH adsorption edges were measured as a function of time, for up to 72 hrs, to verify that 24 hrs was sufficient to allow the

system to reach equilibrium, and to determine the quantity of HMO required for ~100% adsorption of the chromium from solution. The pH adsorption edge methodology is described in detail in the following section. Six of the timed pH adsorption edge experiments were conducted: three at 4, 24, and 48 hours with 10 g/L HMO in 0.001 M $NaNO_3$ and three more experiments were conducted at 24, 48, and 72 hours with 20 g/L HMO in 0.01 M $NaNO_3$. Both groups of experiments contained 10^{-5} M Cr(VI) (Figure 2.3).

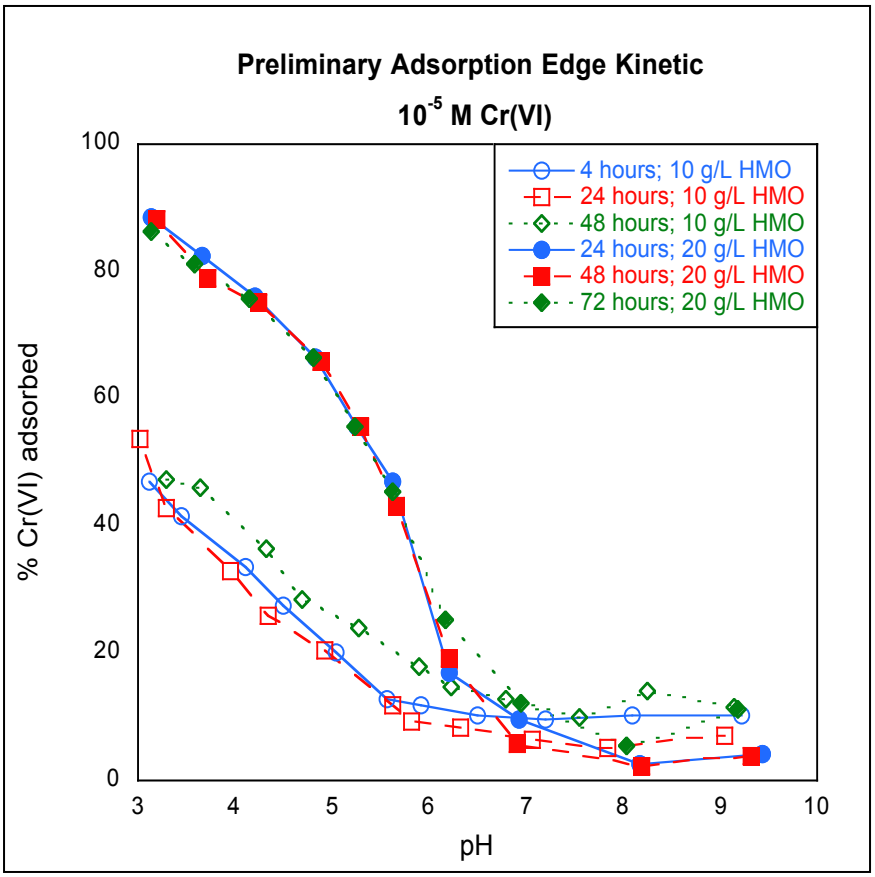

Figure 2.3 Cr(VI) adsorption edges as a function of time.

It was determined that steady state adsorption at a pH of 3 is achieved in 24 hours with 20 g/L HMO. However, comparison of data from all six kinetic experiments suggests that lower concentrations of sorbent will require longer equilibration times. Based on the initial kinetics experiments, it was also determined

that ≥20 g/L HMO is required to achieve ~100% adsorption of a 10^{-5} M Cr(VI) solution at pH ~3.

pH Edge Experiments

Adsorption edge experiments were conducted using 500 mL batch slurries of Cr(VI), $NaNO_3$ and HMO under controlled pCO_2 conditions. The experiments were conducted with concentrations of 20 g/L HMO and either $2 \cdot 10^{-5}$ M or 10^{-5} M Cr. The ionic strength of the experiments was varied from 0.001 M to 0.1 M $NaNO_3$. The pCO_2 was controlled by conducting experiments at the lab bench for atmospheric, inside a Coy glove box for 0% pCO_2, and in a different Coy glove box for elevated pCO_2 of 2.5% and 5%.

To achieve high pCO_2 conditions, concentrated CO_2 was manually introduced into the sealed glove box and the atmospheric concentration in the chamber was measured with a Bacharach CO_2 monitor until the desired pCO_2 concentration was reached. The Bacharach CO_2 monitor was checked periodically to ensure the correct pCO_2 was maintained. Additional CO_2 was titrated in if the measured level of pCO_2 fell below the desired concentration.

To maintain 0% pCO_2 conditions, an airlock was utilized that connects the laboratory to the inside of the glove box. The airlock creates a vacuum of -21 psi three times, flushing with industrial grade nitrogen twice, and a nitrogen/hydrogen gas mix for the final pressure equalization that matches the conditions inside the glove box.

To further maintain correct pCO_2 conditions for both the 0% pCO_2 and the elevated pCO_2 glove boxes, additional inert N_2 gas was titrated into each glove box to slightly higher pressure than the surrounding laboratory. This ensures that any gas exchange that does occur between the glove box and the laboratory is from inside the glove box to outside environment. As an additional precaution to maintain the 0% pCO_2 conditions, a beaker of constantly stirred concentrated LiOH solution, was used

to draw any CO_2 present out of the glove box atmosphere, precipitating it as lithium carbonate.

For each adsorption edge experiment, a 10 mL control aliquot with Cr and $NaNO_3$, prior to addition of the HMO, was removed from each 500 mL batch solution and placed on a rotating lab-quake shaker. 20 g/L HMO was then added to the remaining solution, which was equilibrated under constant mixing for 20 minutes, after which the pH was monitored continuously and titrated down to 3 by drop-wise addition of trace metal grade concentrated nitric acid. At pH 3, a 10 mL aliquot of the slurry was removed, and the pH of the remaining batch was continuously raised by ~0.8 pH intervals, with an aliquot removed and placed on the lab-quake at each pH interval. The titration and removal of aliquots was repeated over a pH spanning ~3 to 10. All aliquots were equilibrated for a further 24 hours, under constant shaking (lab-quake), under the experimental pCO_2. The aliquots were then individually removed from the shaker, the pH of each measured under constant stirring with a magnetic stir bar, and the aliquot replaced on the lab-quake until all aliquots were measured. Finally, all aliquots were removed from the shaker, centrifuged for 20 minutes (under atmospheric conditions) and then quickly syringe-filtered with a 0.2 μm filter into acid-washed, labeled 15 mL centrifuge tubes. Hexavalent chromium in each supernatant was then measured with a UV-Vis spectrophotometer at wavelength 540 nm using the diphenylcarbazide method (Greenberg et al., 1992). Total chromium (Cr(VI) and Cr(III) species) was measured for many of the samples using an inductively coupled plasma optical emission spectrometer (ICP-OES), with matrix-matched calibration standards. Samples were prepared for ICP-OES by combining 5 mL filtered samples with a 1 ppm spike of Y (10 μL of 1000 ppm Y), 5% HNO_3 (714 μL of 70% metal grade HNO_3) and diluting to a total 10 mL (4.276 mL DDI).

CHAPTER III

RESULTS

pH Dependence

All experiments showed that adsorption of Cr(VI) onto HMO is strongly dependent on pH. Adsorption is highest at lower pH values, and decreases with increasing pH. This can be clearly seen in Figure 3.1; nearly 100% of Cr(VI) is sorbed at a pH of 3.0, decreasing to ~4.5% at a pH of 9.8. The pH dependence affecting adsorption is due to the net surface charge of the HMO. The pH_{PPZC} of HMO is low, less than 3, and at low pH the net surface charge is nearly neutral. As pH increases, more surface sites deprotonate giving the HMO surface a stronger net negative charge. The increasingly net negatively charged surface repels and desorbs the negatively charged $HCrO_4^{[-]}$ and $CrO_4^{[-2]}$ aqueous species from the solid surface.

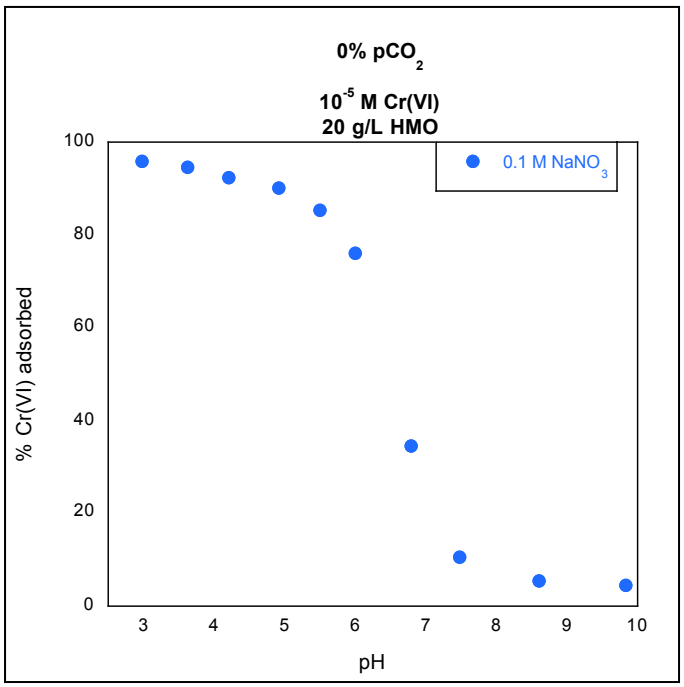

Figure 3.1 Adsorption of 10^{-5} M Cr(VI) on 20 g/L of HMO with 0.1 M $NaNO_3$ and 0% pCO_2.

Ionic Strength Dependence

Adsorption of Cr(VI) on HMO is affected by the ionic strength of the solution, with low ionic strength associated with decreased adsorption and higher ionic strength with increased adsorption. The relationship between the quantity of Cr(VI) sorbed and the ionic strength can be clearly seen in Figure 3.2, and is independent of pCO_2 and pH. The lowest ionic strength experiment (J: 0.001 M $NaNO_3$) has the least adsorption with a maximum of ~55% Cr(VI) sorbed, whereas the highest ionic strength experiment (L: 0.1 M $NaNO_3$) has the greatest Cr(VI) adsorption with nearly 100% of the Cr(VI) sorbed at low pH. The intermediate ionic strength experiment (K: 0.01 M $NaNO_3$) falls between these with a maximum of ~83% Cr(VI) sorbed at low pH.

The ionic strength dependence of Cr(VI) adsorption onto HMO is due to the electrical double layer (edl). The edl originates from the net surface charge of the solid that extends into the solution. Oppositely charged ions in solution are then drawn to this charge, creating a diffuse layer of counter charge. The ionic strength of the solution affects the edl: at a lower ionic strength the edl extends further from the surface, whereas a high ionic strength compresses the edl closer to the solid surface. Presumably, the smaller edl at high ionic strength allows the negatively charged chromate and bichromate ions to more readily approach the surface.

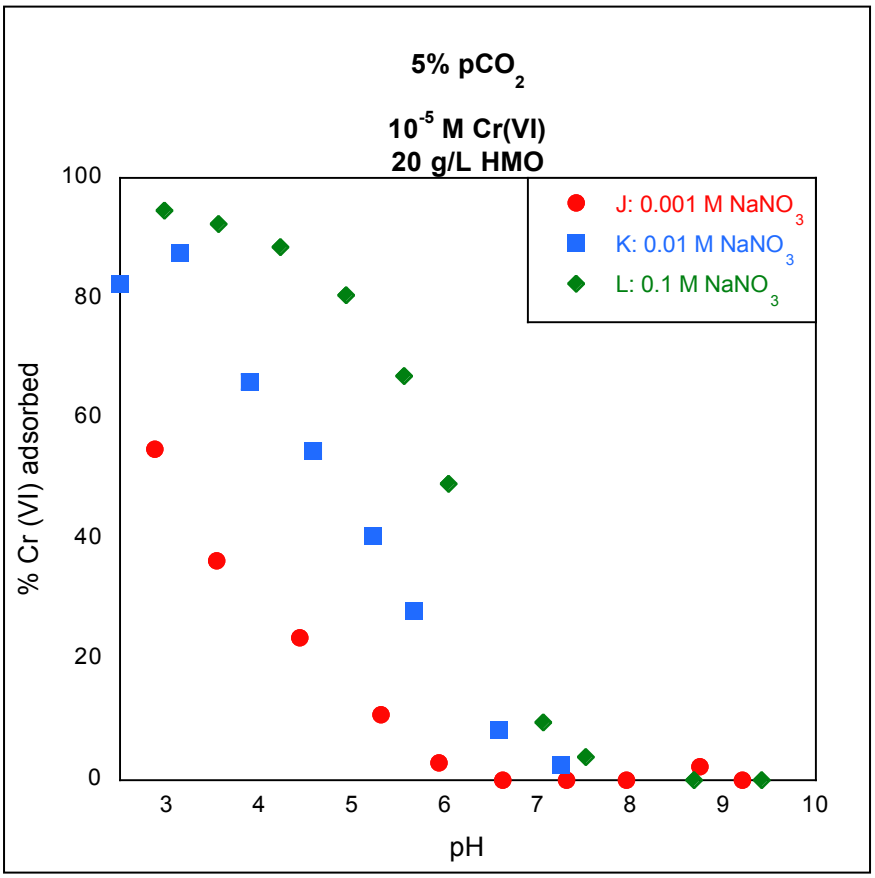

Figure 3.2 Adsorption of 10^{-5} M Cr(VI) on 20 g/L HMO under 5% pCO_2 with 0.001, 0.01 or 0.1 M $NaNO_3$.

pCO_2 Dependence

Cr(VI) adsorption on HMO is also dependent on pCO_2, although to a much lesser extent than the ionic strength dependence (Figures 3.3-3.5). Generally, the 0% pCO_2 experiments are expected to exhibit the greatest percentage of Cr(VI) adsorption followed by atmospheric, 2.5%, and 5% pCO_2, respectively. The reasoning behind this dependence is that carbonate in solution is competing with CrO_4^{-2} to sorb onto surface sites. The greater the pCO_2 of the environment, the more carbonate is in solution competing with chromate and thus less chromate will sorb to the solid. However, in Figure 3.3 and Figure 3.4, the 0% pCO_2 experiments exhibited adsorption significantly less than expected, with edges similar to those for 5% pCO_2

experiments of the same ionic strength. This is likely due to experimental error, and further investigation is required for complete determination of pCO_2 dependence. Figure 3.5 shows 0.1 M $NaNO_3$ experiments that do exhibit the expected order of 0% pCO_2 having the greatest adsorption followed by decreasing levels of adsorption by the atmospheric, 2.5% and 5% pCO_2 respectively.

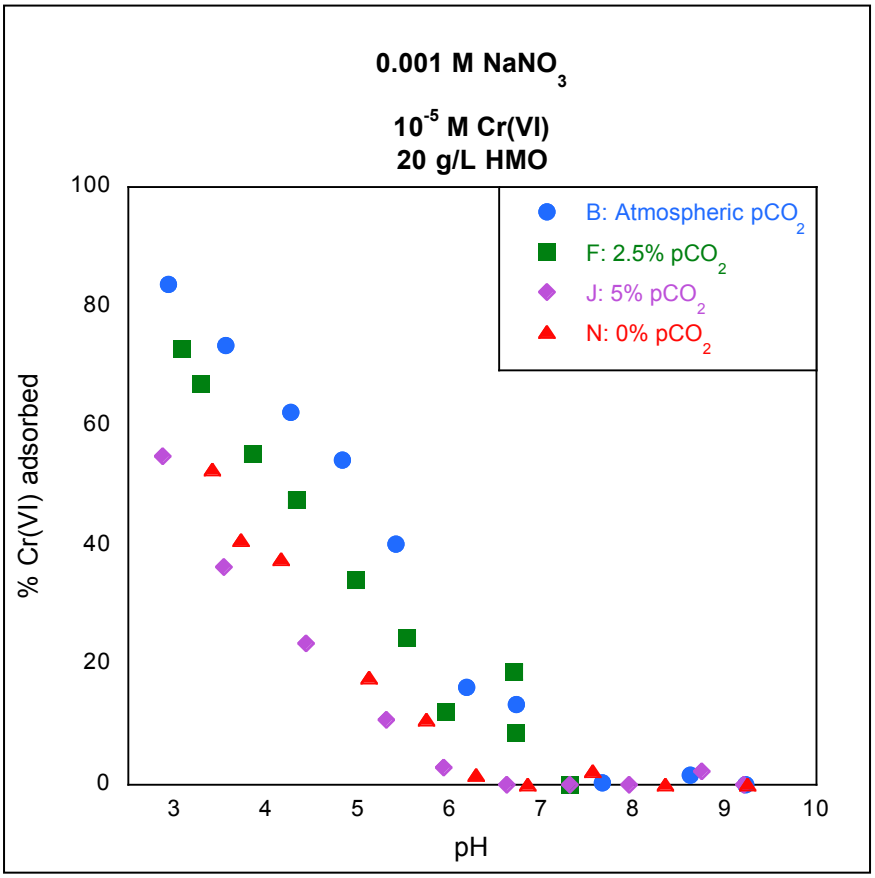

Figure 3.3 Adsorption of 10^{-5} M Cr(VI) on 20 g/L HMO in 0.001 M $NaNO_3$ under varying pCO_2.

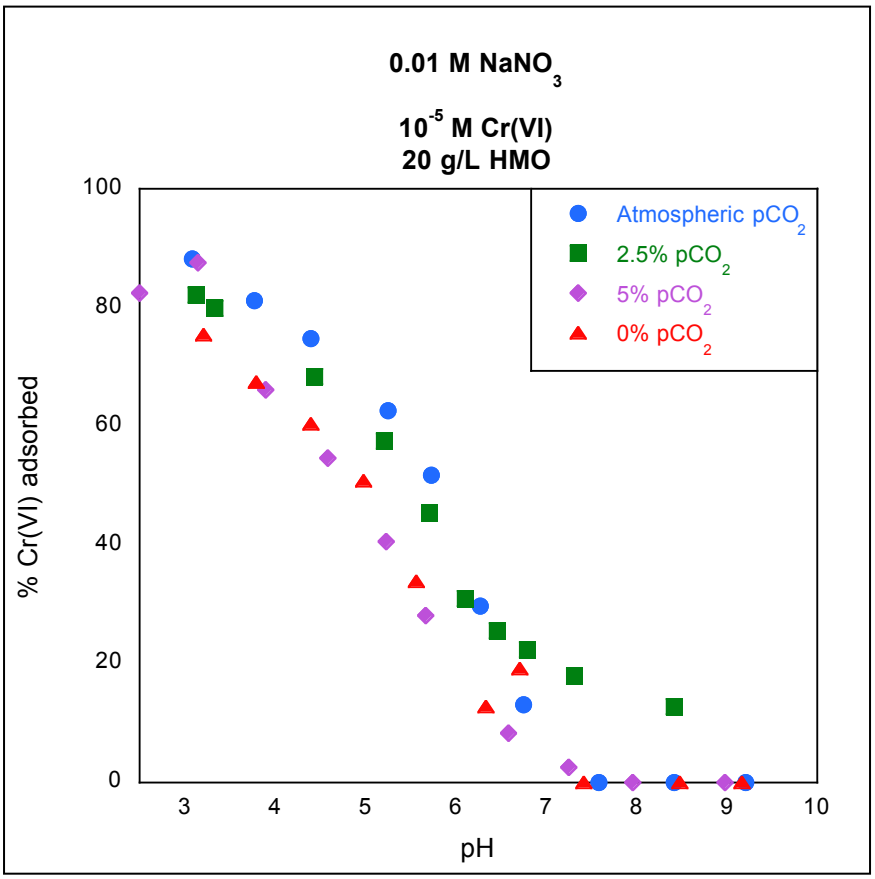

Figure 3.4 Adsorption of 10^{-5} M Cr(VI) on 20 g/L HMO in 0.01 M $NaNO_3$ under varying pCO_2.

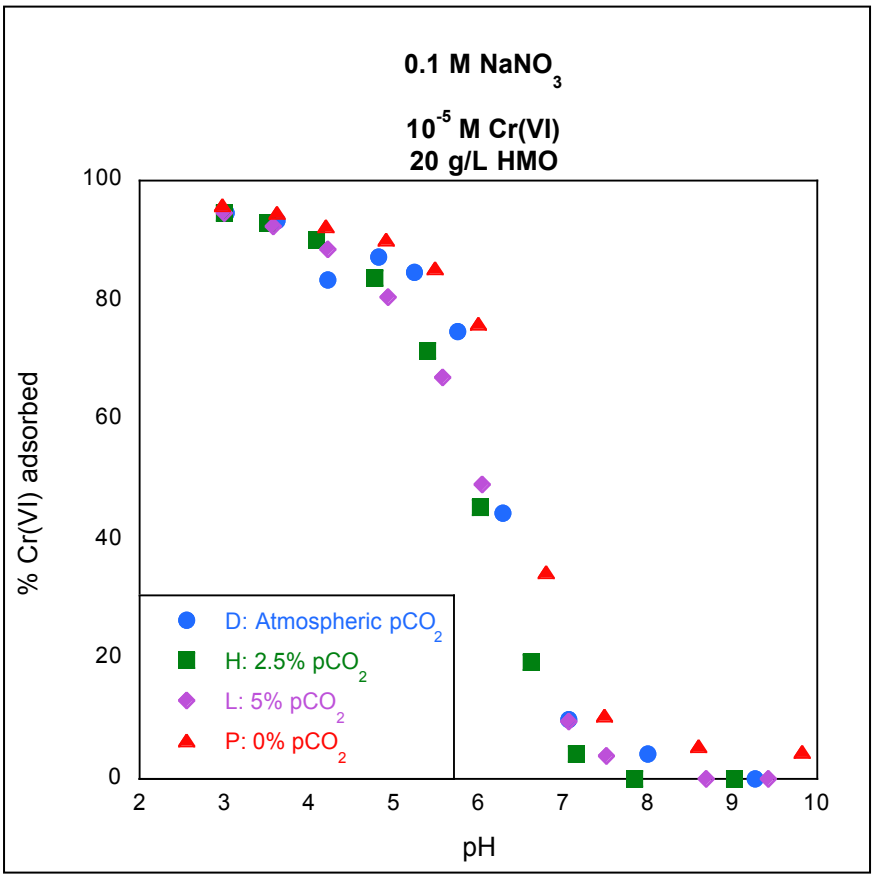

Figure 3.5 Adsorption of 10^{-5} M Cr(VI) on 20 g/L HMO in 0.1 M $NaNO_3$ under varying pCO_2.

Dependence on Sorbate to Sorbent Ratio

The sorbate to sorbent ratio is the Cr(VI) to HMO ratio, and was $1 \cdot 10^{-5}$ M Cr(VI) to 20 g/L HMO. Alternate loadings ($2 \cdot 10^{-5}$ M Cr(VI)) were investigated in two experiments (Q: 0.001 M $NaNO_3$ and R: 0.01 M $NaNO_3$) and showed similar ionic strength and pH dependence (Figures 3.6, 3.7) compared to the $1 \cdot 10^{-5}$ M Cr(VI) loading experiments (J: 0.001 M $NaNO_3$ and K: 0.01 M $NaNO_3$). There is somewhat greater adsorption with the increased Cr(VI) loading with 0.001 M $NaNO_3$, but little change is observed in 0.01 M $NaNO_3$. Alternate loading was only conducted under 5% pCO_2, thus no pCO_2 comparison can be made for this specific loading.

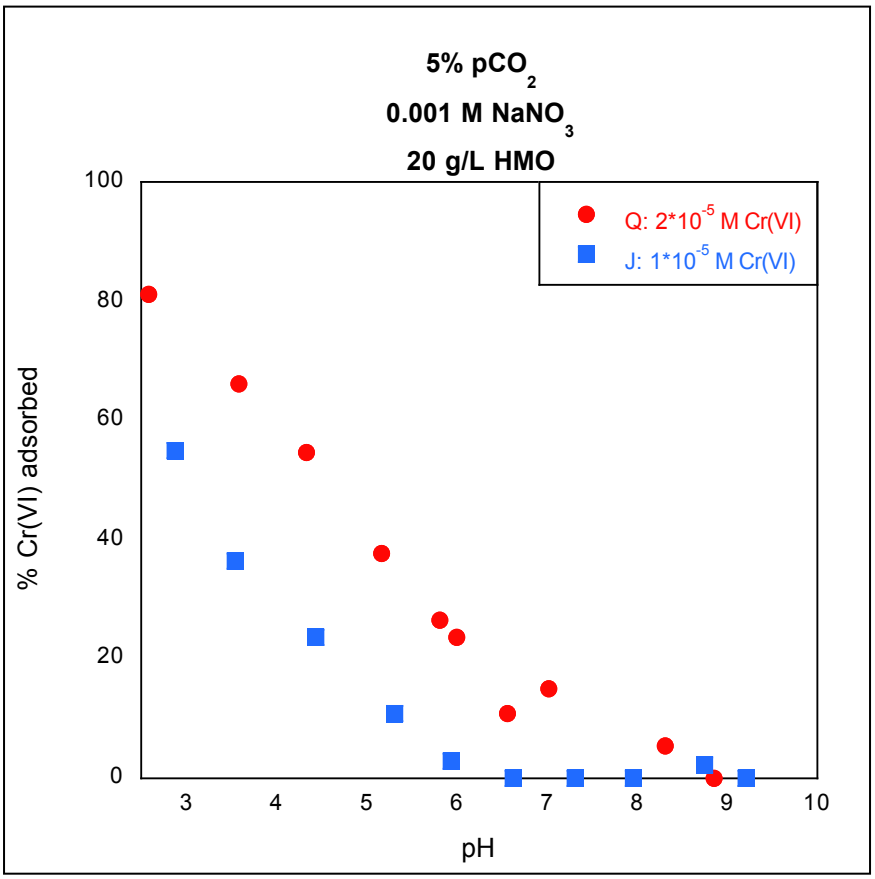

Figure 3.6 Adsorption of $1 \cdot 10^{-5}$ M or $2 \cdot 10^{-5}$ M Cr(VI) on 20 g/L HMO in 0.001 M $NaNO_3$ under 5% pCO_2.

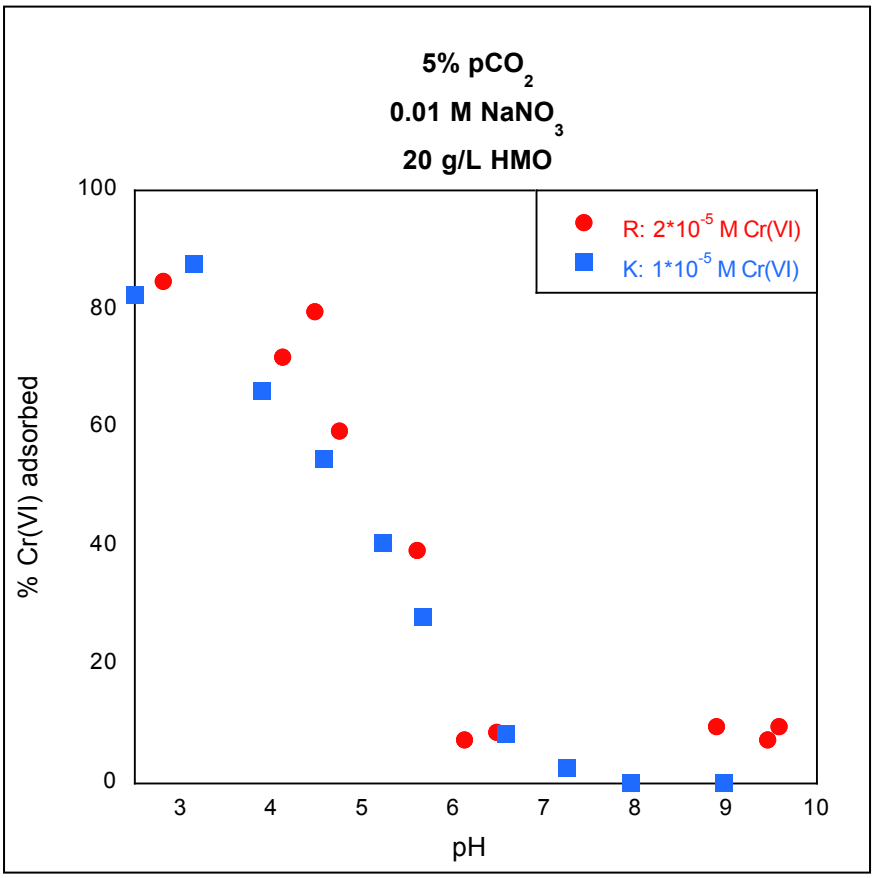

Figure 3.7 Adsorption of $1 \cdot 10^{-5}$ M or $2 \cdot 10^{-5}$ M Cr(VI) on 20 g/L HMO in 0.01 $NaNO_3$ under 5% pCO_2.

CHAPTER IV

DISCUSSION

Surface Complexation Modeling Approach

Cr(VI) adsorption on HMO was measured over a wide variety of solution conditions (pH, pCO_2, ionic strength, sorbate/sorbent ratio) in order to better understand the reactions that occur between Cr(VI) and the HMO surface in natural systems. These data could be used to develop thermodynamic models of the reactions which occur between Cr(VI) and HMO. This is advantageous as measurement of every situation where chromate could sorb is unrealistic and a model gives predictive power for these real world situations. There are many ways to describe adsorption data including empirical methods such as partition coefficients and isotherm equations, however for the greatest predictive power, a surface complexation model (SCM) is optimal because of its ability to predict over varying solution chemistry (Tonkin et al., 2004).

Many different types of thermodynamic SCMs have been developed (e.g. constant capacitance, diffuse layer, triple layer), which mostly differ in their treatment of charge at the solid surface. Although many of these SCMs have been shown to represent a broad range of adsorption data well, to best represent adsorption across multiple sorbing phases, or mixes of solids, model consistency across each phase is required. Dzombak and Morel (1990) developed guidelines for compiling and describing adsorption data for many cations and anions on hydrous ferric oxide (HFO) using a diffuse double layer SCM (DLM). The approach used by Dzombak and Morel (1990) for HFO was adapted by Tonkin et al. (2004) for the development of a DLM to describe cation adsorption on HMO. This was especially desirable because it provided an internally consistent database of complexation constants for ion adsorption on both HMO and HFO, two important constituents, or analogs of constituents, found in many soils and sediments.

The Tonkin et al. (2004) DLM for HMO is particularly useful for this study for several reasons. First, the DLM is included with the default databases of the widely-used thermodynamic speciation code, Visual MINTEQ, and is easy to modify to include other sorbates, such as chromate, beyond the suite of cations investigated by Tonkin et al. (2004). Second, the DLM is consistent with that developed for HFO by Dzombak and Morel (1990) as well as a growing database of minerals that also include goethite (Mathur, 1995) and crystalline Al_2O_3 (Paulson, 1996), thus making the DLM for chromate adsorption onto HMO more useful and easier to apply to real world mineral assemblages than another SCM or empirical methods.

The DLM developed by Tonkin et al. (2004) provides the specific surface area (SSA), site densities, site types, and deprotonation constants that were incorporated into the model developed in this study (for more detail, see Chapter 1). Tonkin et al. (2004) used the theoretically-derived SSA of 746 $m^2\ g^{-1}$. The site densities (number of total surface sites per mole Mn) for HMO were derived by considering the crystallography of Na-birnessite. The total site densities were divided across two site types, >XOH and >YOH, based on best fits to potentiometric titration data from a variety of sources (Tonkin et al., 2004). Finally, acid-dissociation constants for both the surface site types were developed by Tonkin et al. (2004) by fitting existing titration data.

Modeling Cr(VI) Adsorption Under 0% pCO_2

To incorporate chromate into the HMO DLM developed by Tonkin et al. (2004), the stoichiometry of sorbed chromate species and equilibrium stability constants describing the reactions forming each species must be derived. The chromate adsorption complexes were determined by first creating a set of potential chromate reaction stoichiometries to form the following surface complexes: $>SOHCrO_4^{[-2]}$, $>SOH_2CrO_4^{[-1]}$, and $>SOH_3CrO_4$ where >SOH represents either an >XOH or >YOH site. Stability constants were individually optimized for each of the following reactions:

$$>SOH + CrO_4^{[-2]} = >SOHCrO_4^{[-2]} \quad (4.1)$$

$$>SOH + H + CrO_4^{[-2]} = >SOH_2CrO_4^{[-1]} \quad (4.2)$$

$$>SOH + 2H^{[+1]} + CrO_4^{[-2]} = >SOH_3CrO_4 \quad (4.3)$$

using the data from each individual Cr(VI) adsorption edge measured under 0% pCO_2 conditions with the optimization routine in FITEQL (Westall et al, 1980). The 0% pCO_2 edges were used because there is no possibility of competition from carbonate adsorption on the HMO.

The adsorption of Cr(VI) on both the >XOH and >YOH sites was tested by optimizing stability constants for reactions on either >XOH or >YOH sites using the optimization program FITEQL. Of the surface site complexes tested, the $>XOHCrO_4^{[-2]}$ surface complex best fit the experimental adsorption data (Figure 4.1).

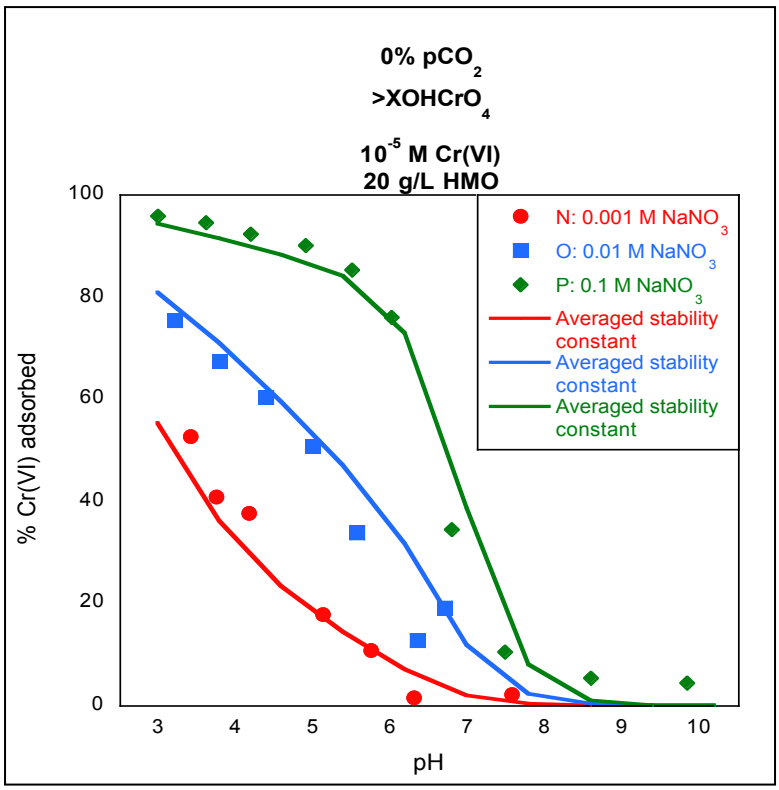

Figure 4.1 Model fits using average of best-fit stability constants, optimized with each individual edge for a reaction 4.1 forming $>XOHCrO_4^{[-2]}$ (see Table 4.2) plotted against experimental data for three adsorption edges.

Next, to see whether a better fit could be obtained, simultaneous adsorption of Cr(VI) on both the >XOH and >YOH sites was tested by simultaneously optimizing stability constants for reactions on the >XOH and >YOH sites using the optimization program FITEQL. Simultaneously optimizing the stability constant values for multiple adsorption reactions is critical because the values are interdependent. Simultaneous optimization of two surface reactions was again completed using each individual 0% pCO_2 adsorption edge.

For each optimization, FITEQL provides a weighted sum of squares over degrees of freedom (WSOS/DF) value; values under 20 are generally assumed to represent a reasonable fit to experimental data (Westall et al. 1980). However, for some of the reactions tested, stability constants could only be optimized for a single experiment or could not be optimized for any experiment, and thus, these combinations of Cr adsorption reactions were not considered further (Table 4.1). For those pairs that did optimize for each 0% pCO_2 adsorption edge, the stability constant values were tabulated and averaged (Table 4.2). The best fit and average stability constants for each pair of chromate surface complexes were then checked by incorporating the reactions and stability constants in the Visual MINTEQ Tonkin DLM thermodynamic database and plotting the calculated adsorption edges against the experimental data (Figure 4.2). The chromate surface complexes that best represented all the experimental data were $>XOHCrO_4^{[-2]}$ and $>YOH_2CrO_4^{[-1]}$ with averaged stability constants of 8.7 and 9.4 respectively (Figure 4.3). It is clear from this figure that simultaneous optimization of stability constants for two surface complexes does not produce better fits than those obtained using only a singl surface complex (Figure 4.1). The chromate surface complexes and their respective stability constants were next applied to experiments conducted under higher pCO_2.

Table 4.1 Reaction stoichiometries not pursued further because insufficient convergence occurred during optimizations of 0% pCO_2 data using FITEQL.

Surface Reaction(s)	Best Fit Log K (WSOS/DF)	Average Log K
$>XOH + CrO_4^{[-2]} = >XOHCrO_4^{[-2]}$	Would not optimize (NA)[a] Would not optimize (NA)[b] Would not optimize (NA)[c]	NA
$>YOH + CrO_4^{[-2]} = >YOHCrO_4^{[-2]}$	Would not optimize (NA)[a] Would not optimize (NA)[b] Would not optimize (NA)[c]	NA
$>XOH + H^{[+1]} + CrO_4^{[-2]} = >XOH_2CrO_4^{[-1]}$	Would not optimize (NA)[a] Would not optimize (NA)[b] 10.3 (0.14)[c]	10.3
$>YOH + H^{[+1]} + CrO_4^{[-2]} = >YOH_2CrO_4^{[-1]}$	Would not optimize (NA)[a] Would not optimize (NA)[b] 10.6 (0.14)[c]	10.6
$>XOH + 2H^{[+1]} + CrO_4^{[-2]} = >XOH_3CrO_4$	Would not optimize (NA)[a] Would not optimize (NA)[b] Would not optimize (NA)[c]	NA
$> YOH + 2H^{[+1]} + CrO_4^{[-2]} = >YOH_3CrO_4$	Would not optimize (NA)[a] Would not optimize (NA)[b] Would not optimize (NA)[c]	

a. Experiment N (0.001 M $NaNO_3$, 20 g/L HMO, 10^{-5} M Cr(VI))

b. Experiment O (0.01 M $NaNO_3$, 20 g/L HMO, 10^{-5} M Cr(VI))

c. Experiment P (0.1 M $NaNO_3$, 20 g/L HMO, 10^{-5} M Cr(VI))

Table 4.2 Reaction stoichiometries considered in this study, with stability constants resulting from optimization using 0% pCO_2 data with FITEQL.

Surface Reaction(s)	Best Fit Log K (WSOS/DF)	Average Log K
$>XOH + CrO_4^{[-2]} = >XOHCrO_4^{[-2]}$	8.60 (0.11)[a] 9.09 (0.14)[b] 8.00 (0.18)[c]	8.57
$>XOH + H^{[+1]} + CrO_4^{[-2]} =$ $>XOH_2CrO_4^{[-1]}$	10.21 (0.3)[a] 11.05 (1.25)[b] 12.52 (0.66)[c]	11.3
$>YOH + CrO_4^{[-2]} = >YOHCrO_4^{[-2]}$	8.66 (0.84)[a] 9.03 (1.88)[b] 7.07 (18.2)[c]	8.3
$>YOH + H^{[+1]} + CrO_4^{[-2]} =$ $>YOH_2CrO_4^{[-1]}$	10.4 (0.2)[a] 11.15 (0.78)[b] 10.58 (0.12)[c]	10.7
$>XOH + 2H^{[+1]} + CrO_4^{[-2]} =$ $>XOH_3CrO_4$	11.71 (0.77)[a] 13.05 (2.55)[b] Would not optimize (NA)[c]	12.4
$>YOH + 2H^{[+1]} + CrO_4^{[-2]} =$ $>YOH_3CrO_4$	11.91 (0.69)[a] 13.14 (2.21)[b] 15.15 (0.69)[c]	13.4
$>XOH + CrO_4^{[-2]} = >XOHCrO_4^{[-2]}$	8.39 (0.06)[a] 9.09 (0.16)[b] Would not optimize (NA)[c]	8.7
$>YOH + H^{[+1]} + CrO_4^{[-2]} =$ $>YOH_2CrO_4^{[-1]}$	10 (0.06)[a] 8.89 (0.16)[b] Would not optimize (NA)[c]	9.4
$>XOH + H^{[+1]} + CrO_4^{[-2]} =$ $>XOH_2CrO_4^{[-1]}$	10.07 (0.17)[a] 10.75 (0.76)[b] 12.06 (0.35)[c]	11.0
$>YOH + CrO_4^{[-2]} = >YOHCrO_4^{[-2]}$	8.19 (0.17)[a] 8.67 (0.76)[b]	7.4

	5.38 (0.35)[c]	

a. Experiment N (0.001 M $NaNO_3$, 20 g/L HMO, 10^{-5} M Cr(VI))

b. Experiment O (0.01 M $NaNO_3$, 20 g/L HMO, 10^{-5} M Cr(VI))

c. Experiment P (0.1 M $NaNO_3$, 20 g/L HMO, 10^{-5} M Cr(VI))

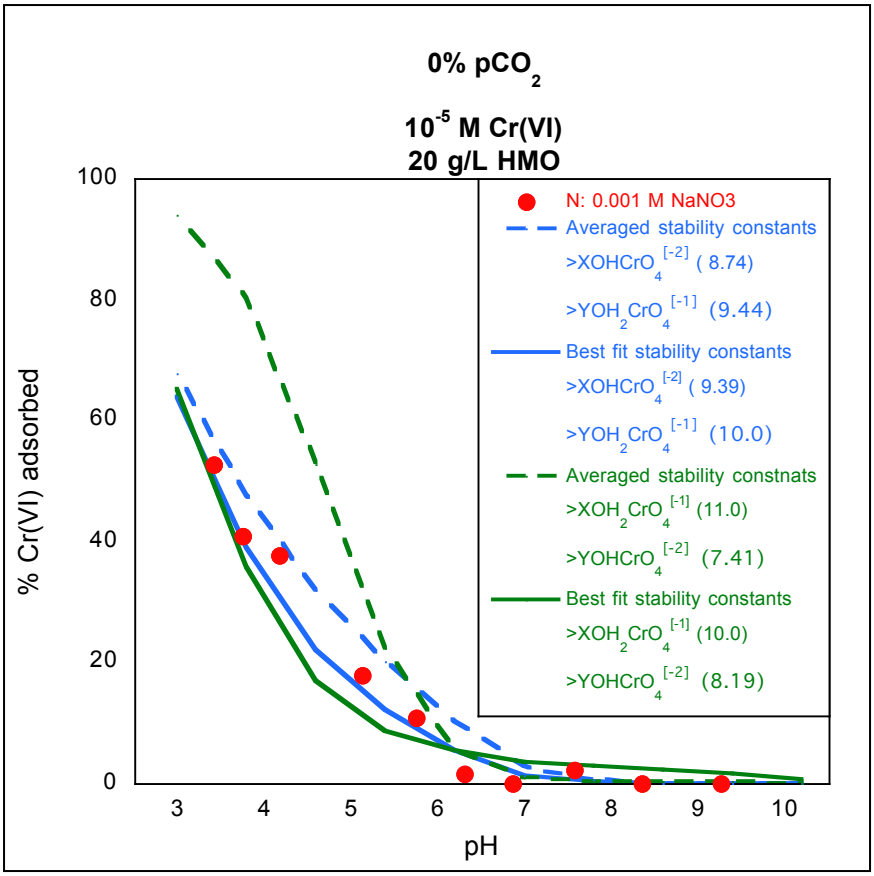

Figure 4.2 Example of model fits based on average and best-fit stability constants, derived for two sets of simultaneously optimized reaction stoichiometries (forming $>XOHCrO_4^{[-2]}$ and $>YOH_2CrO_4^{[-1]}$ or $>XOH_2CrO_4^{[-1]}$ and $>YOHCrO_4^{[-2]}$, see Table 4.2) plotted against experimental data for one adsorption edge.

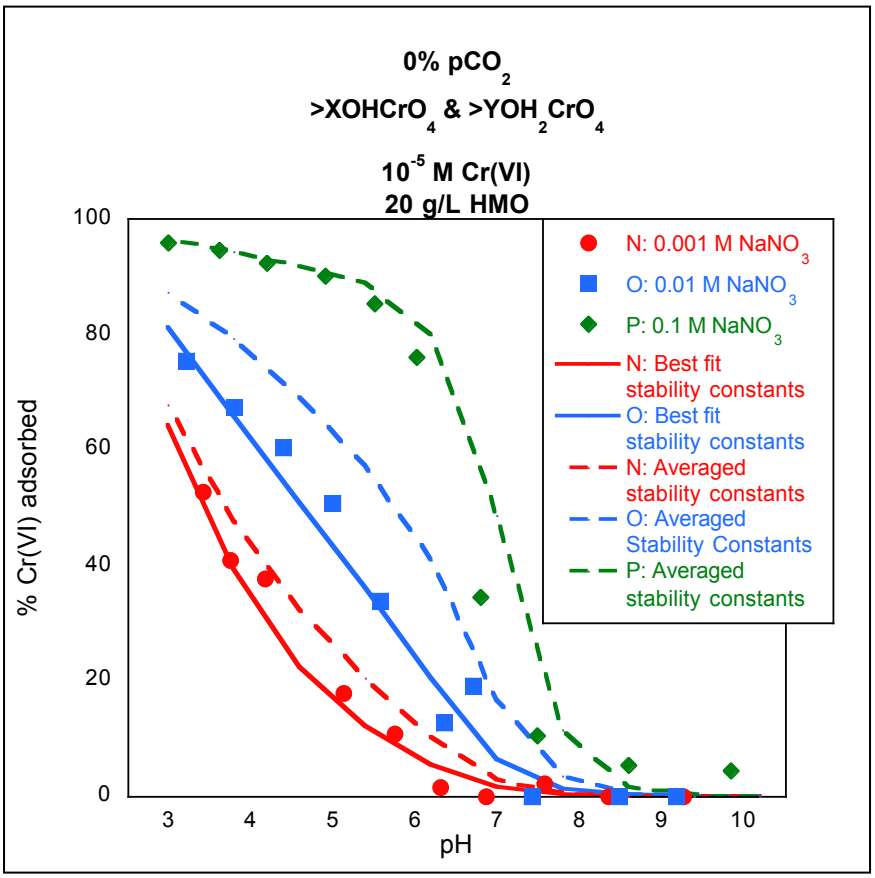

Figure 4.3 Model fits using averaged and best-fit stability constants (Table 4.2) derived for $>XOHCrO_4^{[-2]}$ and $>YOH_2CrO_4^{[-1]}$ surface complexes compared to experimental data (0.001, 0.01, and 0.1 M $NaNO_3$ experiments at 0% pCO_2).

Modeling Cr(VI) Adsorption Under Elevated pCO_2

The chromate surface complexes and their respective stability constants developed for 0% pCO_2 conditions were used to predict adsorption edges for experiments conducted with pCO_2 present. The single $>XOHCrO_4^{[-2]}$ surface complex model fits the experimental data fairly well, without the addition of a carbonate surface species. However, adsorption of Cr(VI) at 0.1 M NaNO3 is over predicted (Figure 4.3), suggesting that a better fit might be obtained with the addition of a carbonate surface complex. To test this notion, and to try to achieve a better fit for

the single $>XOHCrO_4^{[-2]}$ surface complex model, carbonate surface complexes were included in the models, and the experimental data used to derive best-fit stability constants describing formation of these complexes. This was accomplished similarly to derivation of the best-fit chromate surface complexes, by optimizing for the stability constants describing reactions to form carbonate surface complexes using data for 5% pCO_2 conditions with the optimization program FITEQL. The 5% pCO_2 experimental conditions were chosen because these are expected to have the greatest concentration of carbonate in solution and, thus, the influence of carbonate competition with chromate should be the greatest. The carbonate surface complexes were determined by first creating a set of potential carbonate reaction stoichiometries to form the following surface complexes: $>SOHCO_3^{[-2]}$ and $>SOH_2CO_3^{[-1]}$, where >SOH represents either an >XOH or >YOH site. Stability constants were individually optimized for each of the following reactions:

$$>SOH + CO_3^{[-2]} = >SOHCO_3^{[-2]} \quad (4.4)$$

$$>SOH + H^{[+1]} + CO_3^{[-1]} = >SOH_2CO_3^{[-1]} \quad (4.5)$$

using the data from each individual adsorption edge measured under 5% pCO_2 conditions and inputting the total dissolved carbonate as a function of pH calculated from Visual MINTEQ with the optimization routine in FITEQL (Westall et al, 1980). In combination with the single $>XOHCrO_4^{[-2]}$ surface complex, optimizations using all but one of the carbonate reactions converged in the optimization program FITEQL (Table 4.3; Table 4.4; Figure 4.4). The best fit was produced with the addition of a $>YOH_2CO_3^{[-1]}$ complex. The DLM derived for chromate adsorption onto HMO in the presence of high pCO_2 ($>XOHCrO_4^{[-2]}$ and $>YOH_2CO_3^{[-2]}$ with log stability constants 8.57, and 17.17 respectively) under predicts Cr(VI) adsorption for the 0.001 M $NaNO_3$ experiments for both atmospheric (Figure 4.5) and 2.5% (Figure 4.6) pCO_2 conditions. The DLM over predicts Cr(VI) adsorption for 0.1 M $NaNO_3$ for atmospheric pCO_2 and underestimates at low pH and overestimates at high pH the 0.1 M $NaNO_3$ for 2.5% pCO_2 experiment fairly well. The presence of the carbonate adsorption species appears to have very little influence in the atmospheric pCO_2

experiments and slightly more influence in the 2.5% pCO_2 experiments, notably experiment H (0.1 M $NaNO_3$) and experiment G (0.01 M $NaNO_3$). The 5% pCO_2 experiments were the most affected by the presence of carbonate (Figure 4.3).

Table 4.3 Carbonate reaction stochiometries considered in this study with resulting stability constants optimized using FITEQL with Cr(VI) edges collected under 5% pCO_2 for $>XOHCrO_4^{[-2]}$.

$>XOH + CO_3^{[-2]} = >XOHCO_3^{[-2]}$	17.51 (0.21)[a] 14.95 (0.96)[b] Would not optimize (NA)[c]	16.2
$>XOH + H^{[+1]} + CO_3^{[-2]]} = >XOH_2CO_3^{[-1]}$	16.48 (0.23)[a] Would not optimize (NA)[b] 19.95 (3.79)[c]	18.2
$>YOH + H^{[+1]} + CO_3^{[-2]} = >YOH_2CO_3^{[-1]}$	16.54 (0.23)[a] 17.79 (1.48)[b] Would not optimize (NA)[c]	17.17

a. Experiment J (0.001 M $NaNO_3$, 20 g/L HMO, 10^{-5} M Cr(VI))
b. Experiment K (0.01 M $NaNO_3$, 20 g/L HMO, 10^{-5} M Cr(VI))
c. Experiment L (0.1 M $NaNO_3$, 20 g/L HMO, 10^{-5} M Cr(VI))

Table 4.4 Carbonate reaction stochiometries not considered further in this study because stability constants could not be optimized using FITEQL using the Cr(VI) adsorption data collected under 5% pCO_2 for $>XOHCrO_4^{[-2]}$ and $>YOH_2CrO_4^{[-1]}$.

$>XOH + CO_3^{[-2]} = >XOHCO_3^{[-2]}$	Would not optimize (NA)[a] 15.1 (0.88)[b] Would not optimize (NA)[c]	15.1

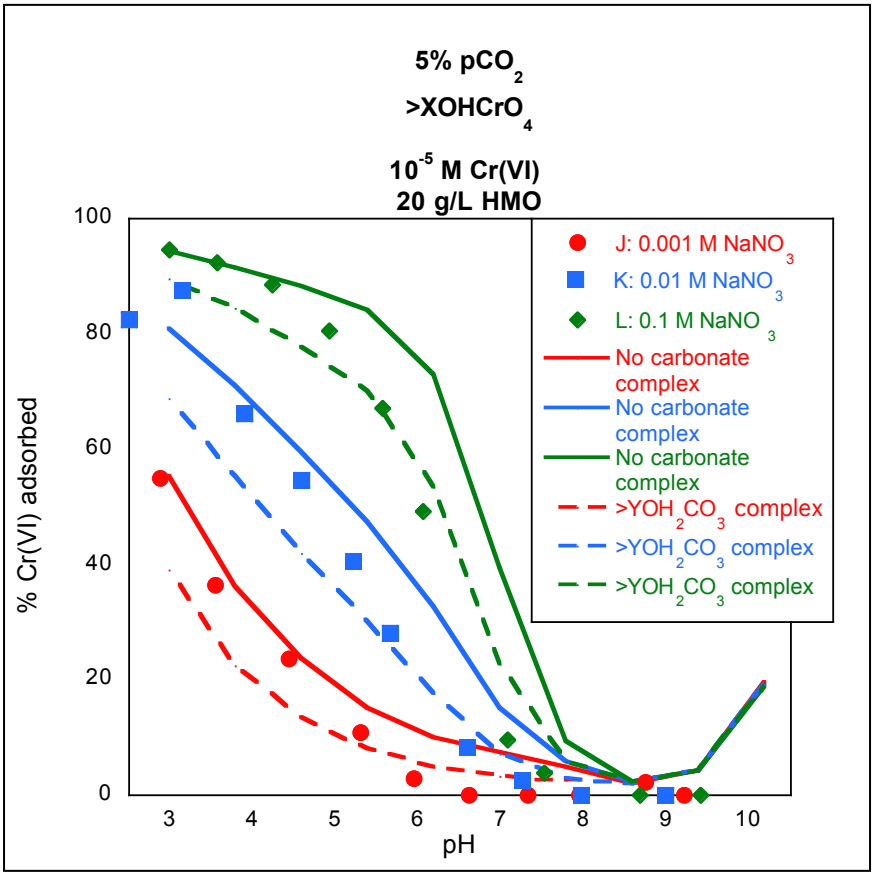

Figure 4.4 Calculated Cr(VI) adsorption without the carbonate complex, $>XOHCrO_4^{[-2]}$ (8.57; solid lines), compared to fits using the carbonate complex $>YOH_2CO_3^{[-2]}$ (17.17; dashed line); the average log stability constants were derived based on optimization of each of the three edges using FITEQL (see Table 4.3).

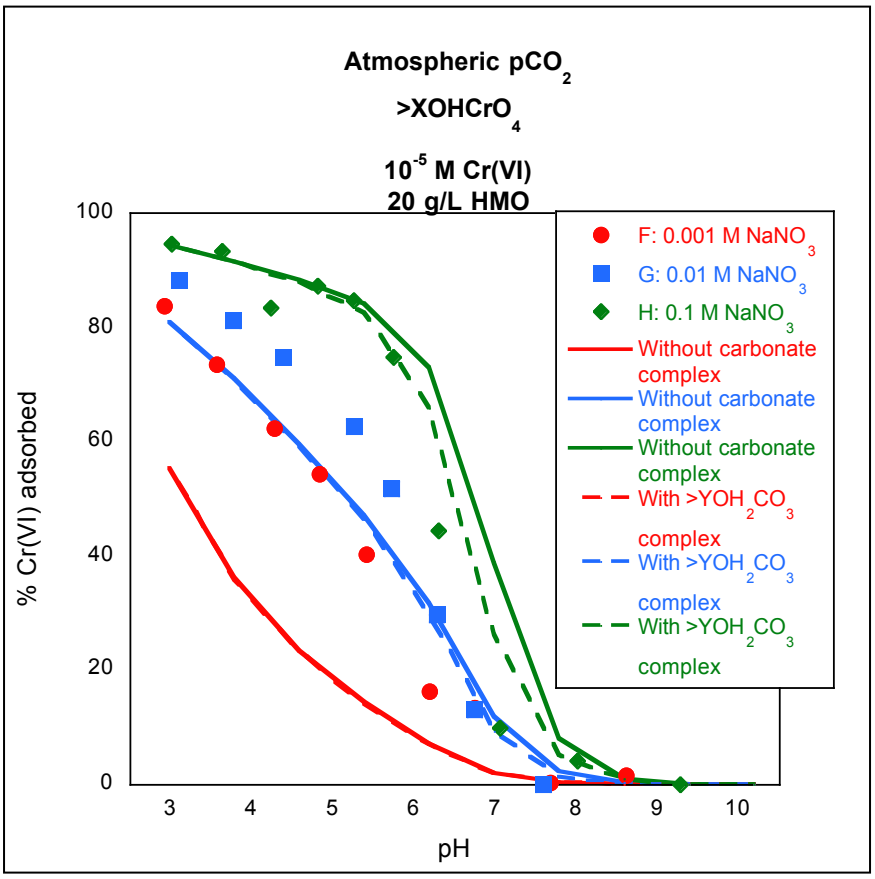

Figure 4.5 Calculated Cr(VI) adsorption for atmospheric pCO_2 experiments based on log stability constants for the carbonate complex, $>YOH_2CO_3^{[-1]}$ (17.17; dashed lines), derived by averaging carbonate optimizations for 0.001, 0.01, and 0.1 M $NaNO_3$ experiments at 5% pCO_2 using MINTEQ, compared to fits without the carbonate complex (solid lines) derived using FITEQL. Log stability constants for formation of $>XOHCrO_4^{[-2]}$ were set to 8.57 for all calculations.

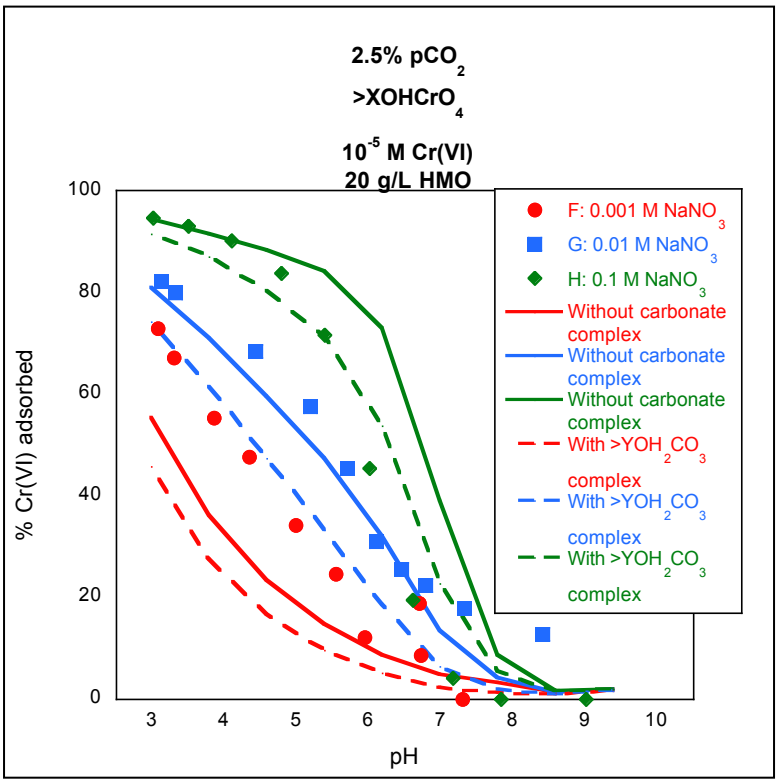

Figure 4.6 Calculated Cr(VI) adsorption for 2.5% pCO_2 experiments based on log stability constants for the carbonate complex, $>YOH_2CO_3^{[-1]}$ (17.17; dashed lines) , derived by averaging for 0.001, 0.01, and 0.1 M $NaNO_3$ experiments at 5% pCO_2 using MINTEQ, compared to fits without the carbonate complex (solid lines) derived using FITEQL. Log stability constants for formation of $>XOHCrO_4^{[-2]}$ were set to 8.57.

The addition of carbonate species was also tested in combination with the model including two chromate surface species ($>XOHCrO_4^{[-2]}$ and $>YOH_2CrO_4^{[-1]}$). However, it was not possible to optimize stability constants for many of the carbonate reactions (FITEQL did not converge), or optimization was possible for only one experiment, or WSOS/DF were very high, indicating a poor fit to the experimental data (Table 4.5). This left only one complex that fit the parameters to be used, $>XOHCO_3^{[-2]}$ (Table 4.6) with an averaged (from 0.001, 0.01, and 0.1 M $NaNO_3$ edges) log stability constant for formation of 12.0 (Figure 4.7).

Table 4.5 Carbonate reaction stochiometries not considered further in this study because stability constants could not be optimized using FITEQL using the Cr(VI) adsorption data collected under 5% pCO_2 for $>XOHCrO_4^{[-2]}$ and $>YOH_2CrO_4^{[-1]}$.

$>YOH + CO_3^{[-2]} = >YOHCO_3^{[-2]}$	Would not optimize (NA)[a] Would not optimize (NA)[b] Would not optimize (NA)[c]	NA
$>XOH + H^{[+1]} + CO_3^{[-2]]} = >XOH_2CO_3^{[-1]}$	Would not optimize (NA)[a] Would not optimize (NA)[b] 15.53 (13.76)[c]	15.5
$>YOH + H^{[+1]} + CO_3^{[-2]} = >YOH_2CO_3^{[-1]}$	15.10 (44.57)[a] 15.0 (31.31)[b] Would not optimize (NA)[c]	15.1
$>XOH + CO_3^{[-2]} = >XOHCO_3^{[-2]}$ $>YOH+ CO_3^{[-2]} = >YOHCO_3^{[-2]}$	Would not optimize (NA)[a] Would not optimize (NA)[b] Would not optimize (NA)[c] Would not optimize (NA)[a] Would not optimize (NA)[b] Would not optimize (NA)[c]	NA
$>XOH + CO_3^{[-2]} = >XOHCO_3^{[-2]}$ $>YOH + H^{[+1]} + CO_3^{[-2]} = >YOH_2CO_3^{[-1]}$	Would not optimize (NA)[a] Would not optimize (NA)[b] Would not optimize (NA)[c] Would not optimize (NA)[a] Would not optimize (NA)[b] Would not optimize (NA)[c]	NA
$>XOH + H^{[+1]} + CO_3^{[-2]} = >XOH_2CO_3^{[-1]}$ $>YOH + CO_3^{[-2]} = >YOH_2CO_3^{[-1]}$	Would not optimize (NA)[a] Would not optimize (NA)[b] Would not optimize (NA)[c] Would not optimize (NA)[a] Would not optimize (NA)[b] Would not optimize (NA)[c]	NA

a. Experiment J (0.001 M $NaNO_3$, 20 g/L HMO, 10^{-5} M Cr(VI))

b. Experiment K (0.01 M $NaNO_3$, 20 g/L HMO, 10^{-5} M Cr(VI))

c. Experiment L (0.1 M $NaNO_3$, 20 g/L HMO, 10^{-5} M Cr(VI))

Table 4.6 Carbonate reaction stochiometries considered in this study with resulting stability constants optimized using FITEQL with Cr(VI) edges collected under 5% pCO_2 for $>XOHCrO_4^{[-2]}$ and $>YOH_2CrO_4^{[-1]}$.

$>XOH + CO_3^{[-2]} = >XOHCO_3^{[-2]}$	Would not optimize (NA)[a] 12.47 (0.32)[b] 11.43 (0.23)[c]	12.0

a. Experiment J (0.001 M $NaNO_3$, 20 g/L HMO, 10^{-5} M Cr(VI))

b. Experiment K (0.01 M $NaNO_3$, 20 g/L HMO, 10^{-5} M Cr(VI))‹

c. Experiment L (0.1 M $NaNO_3$, 20 g/L HMO, 10^{-5} M Cr(VI))

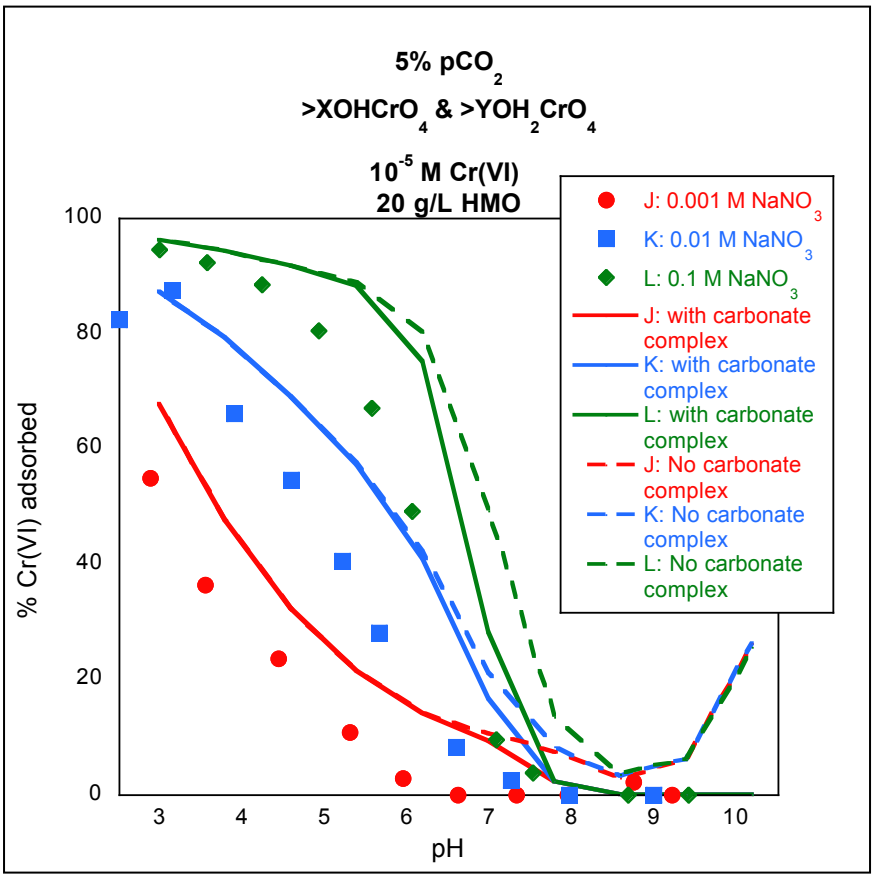

Figure 4.7 Calculated Cr(VI) adsorption without the carbonate complex, $>XOHCrO_4^{[-2]}$ (dashed lines), compared to fits using the average log stability constant (12.0; solid lines) derived for the three ionic strengths using FITEQL (see Table 4.5). Log stability constants for formation of $XOHCrO_4^{[-2]}$ and $>YOH_2CrO_4^{[-1]}$ were set to 8.7 and 9.4 for all calculations.

The DLM derived for chromate adsorption onto HMO in the presence of high pCO_2 ($>XOHCrO_4^{[-2]}$, $>YOH_2CrO_4^{[-1]}$ and $>XOHCO_3^{[-2]}$ with log stability constants 8.7, 9.4, and 12.0 respectively) under predicts Cr(VI) adsorption for the 0.001 M $NaNO_3$ experiments for both atmospheric (Figure 4.8) and 2.5% (Figure 4.9) pCO_2 conditions. The DLM over predicts Cr(VI) adsorption for 0.1 M $NaNO_3$ for both the atmospheric and 2.5% pCO_2 experiments. The presence of the carbonate adsorption species appears to have very little influence in the atmospheric pCO_2 experiments and

slightly more influence in the 2.5% pCO_2 experiments, notably experiment H (0.1 M $NaNO_3$) and in the upper pH range of experiment G (0.01 M $NaNO_3$). The 5% pCO_2 experiments were the most affected by the presence of carbonate (Figure 4.7).

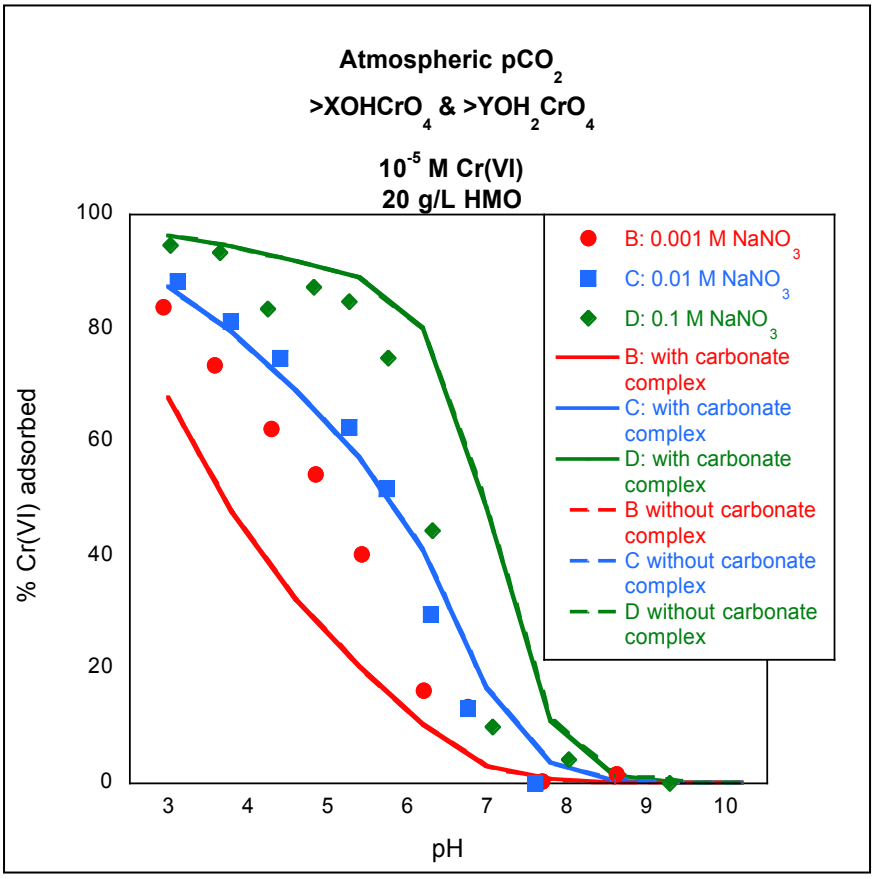

Figure 4.8 Calculated Cr(VI) adsorption for atmospheric pCO_2 experiments based on log stability constants for the carbonate complex, $>XOHCO_3^{[-2]}$ (12.0; solid lines), derived by averaging carbonate optimizations for 0.001, 0.01, and 0.1 M $NaNO_3$ experiments at 5% pCO_2 using MINTEQ, compared to fits without the carbonate complex (dashed lines) derived using FITEQL. Log stability constants for formation of $>XOHCrO_4^{[-2]}$ and $>YOH_2CrO_4^{[-1]}$ were set to 8.7 and 9.4 for all calculations.

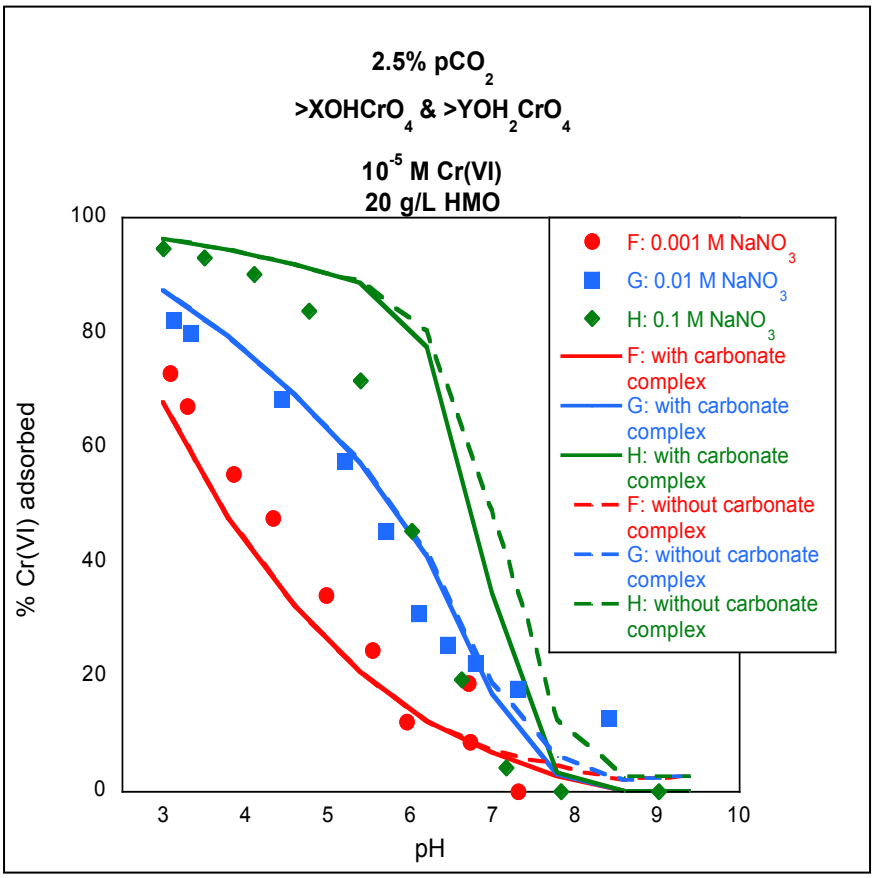

Figure 4.9 Calculated Cr(VI) adsorption for 2.5% pCO_2 experiments based on log stability constants for the carbonate complex, $>XOHCO_3^{[-2]}$ (12.0; solid lines) , derived by averaging for 0.001, 0.01, and 0.1 M $NaNO_3$ experiments at 5% pCO_2 using MINTEQ, compared to fits without the carbonate complex (dashed lines) derived using FITEQL. Log stability constants for formation of $>XOHCrO_4^{[-2]}$ and $>YOH_2CrO_4^{[-1]}$ were set to 8.7 and 9.4 for all calculations.

Effect of Sorbate to Sorbent Ratio: Model Predictions & Experimental Results

A robust DLM should be able to correctly predict adsorption under a variety of sorbate to sorbent ratios. The DLM derived as described above for experiments with 20 g/L HMO and 10^{-5} M Cr(VI), was therefore used to predict chromate adsorption with an alternate loading of $2 \cdot 10^{-5}$ M Cr(VI) onto 20 g/L. The single chromate surface model ($>XOHCrO_4^{[-2]}$ (8.57) and $>YOH_2CO_3^{[-1]}$ (17.17)) under

predicts Cr(VI) adsorption compared to the 0.001 M $NaNO_3$ experimental data (Figure 4.10) and describes Cr(VI) adsorption fairly well compared to the 0.01 M $NaNO_3$ experimental data (Figure 4.11).

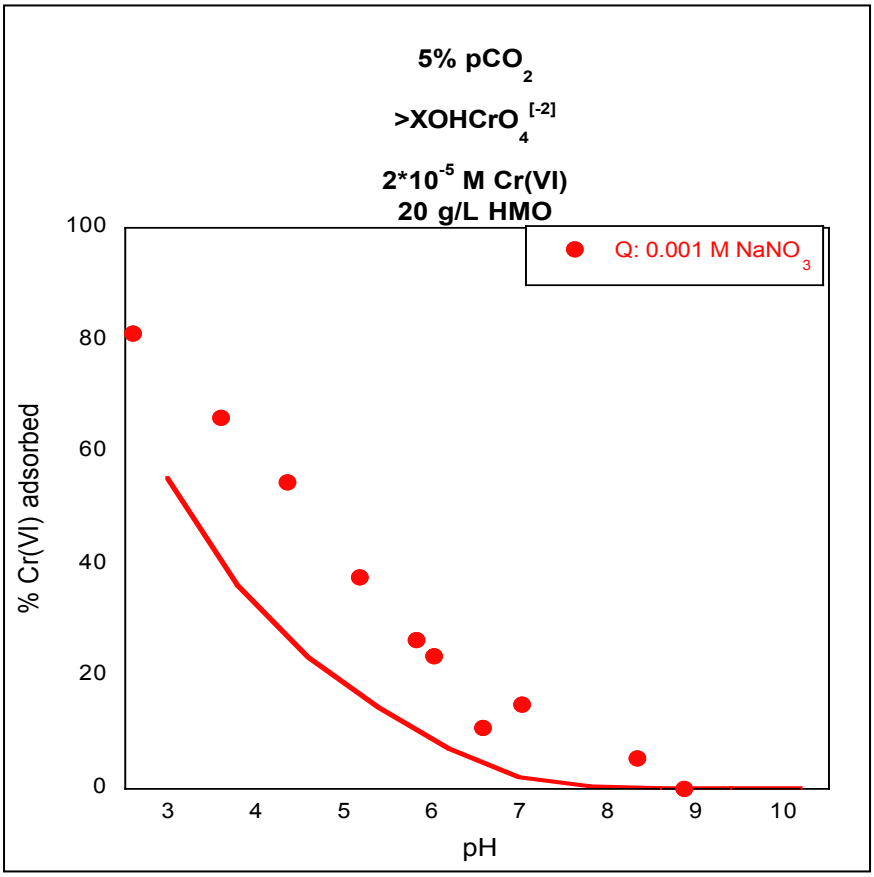

Figure 4.10 Calculated Cr(VI) adsorption for 0.001 M $NaNO_3$ experiment using alternate loading of $2 \cdot 10^{-5}$ M Cr(VI) onto 20 g/L based on log stability constants for the carbonate complex, $>XOHCO_3^{[-2]}$ (17.17; solid lines), derived by averaging 0.001, 0.01, and 0.1 M $NaNO_3$ experiments at 5% pCO_2 using MINTEQ, compared to experimental data. Log stability constants for formation of $>XOHCrO_4^{[-2]}$ were set to 8.57 for all calculations.

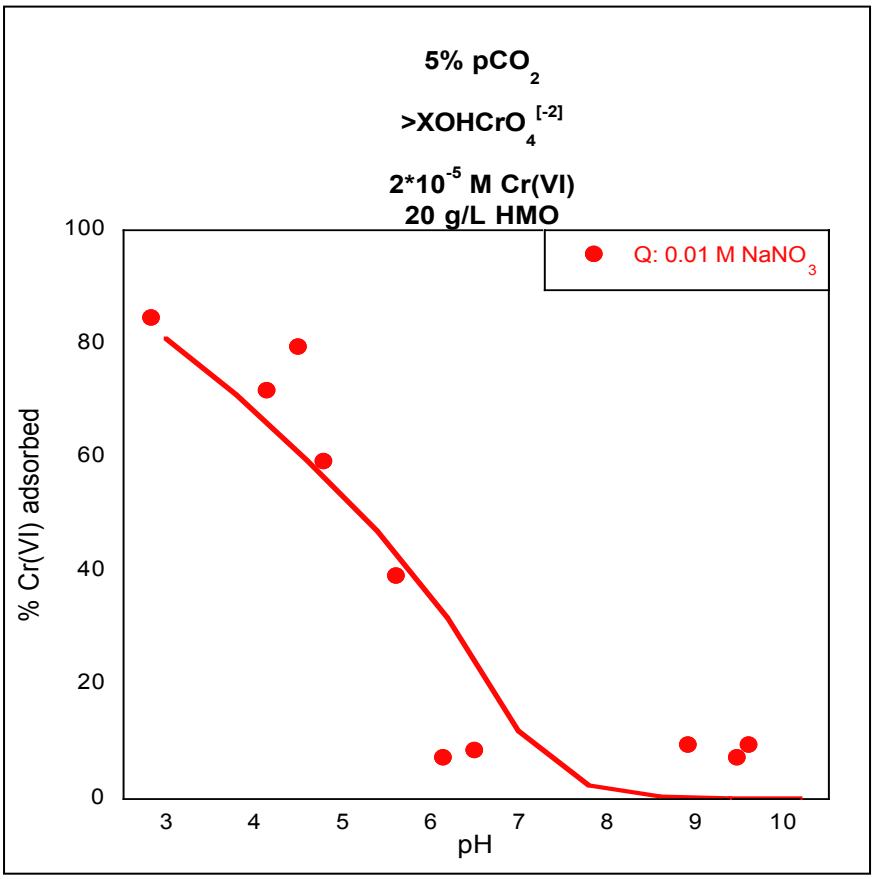

Figure 4.11 Calculated Cr(VI) adsorption for 0.01 M $NaNO_3$ experiment using alternate loading of $2 \cdot 10^{-5}$ M Cr(VI) onto 20 g/L based on log stability constants for the carbonate complex, $>XOHCO_3^{[-2]}$ (17.17; solid lines), derived by averaging 0.001, 0.01, and 0.1 M $NaNO_3$ experiments at 5% pCO_2 using MINTEQ, compared to experimental data. Log stability constants for formation of $>XOHCrO_4^{[-2]}$ were set to 8.57 for all calculations.

The model with two chromate surface complexes ($>XOHCrO_4^{[-2]}$ (8.7), $>YOH_2CrO_4^{[-1]}$ (9.4), and $>XOHCO_3^{[-2]}$ (12.0)) slightly over predicts Cr(VI) adsorption at lower pH for the 0.01 M $NaNO_3$ experimental data (Figure 4.12) and underestimates Cr(VI) adsorption compared to the 0.001 M $NaNO_3$ experimental data (Figure 4.13). It is not clear whether these discrepancies are due to experimental error

(as evidenced by the significant scatter in the experimental data) or indicates that the model needs to be improved.

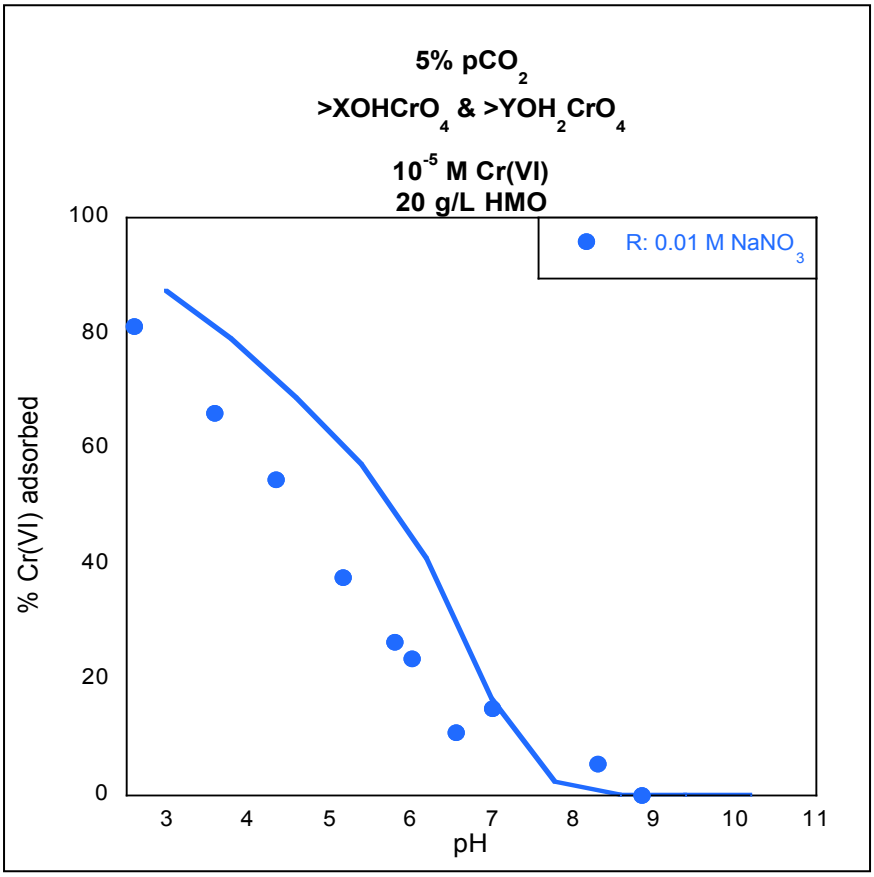

Figure 4.12 Calculated Cr(VI) adsorption for 0.01 M $NaNO_3$ experiment using alternate loading of $2 \cdot 10^{-5}$ M Cr(VI) onto 20 g/L based on log stability constants for the carbonate complex, $>XOHCO_3^{[-2]}$ (12.0; solid lines), derived by averaging 0.001, 0.01, and 0.1 M $NaNO_3$ experiments at 5% pCO_2 using MINTEQ, compared to experimental data. Log stability constants for formation of $>XOHCrO_4^{[-2]}$ and $>YOH_2CrO_4^{[-1]}$ were set to 8.7 and 9.4 for all calculations.

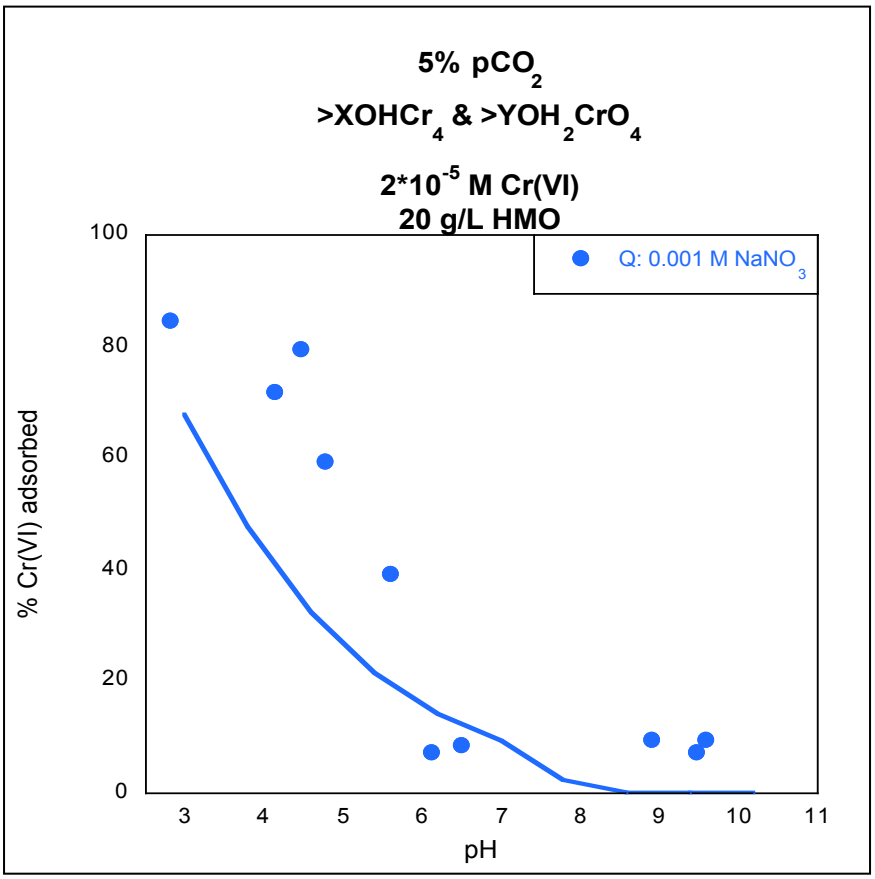

Figure 4.13 Calculated Cr(VI) adsorption of 0.001 M $NaNO_3$ experiment for alternate loading experiment of $2 \cdot 10^{-5}$ M Cr(VI) onto 20 g/L based on log stability constants for the carbonate complex, $>XOHCO_3^{[-2]}$ (12.0; solid lines), derived by manually fitting for 0.001, 0.01, and 0.1 M $NaNO_3$ experiments at 5% pCO_2 using MINTEQ, compared to experimental data. Log stability constants for formation of $>XOHCrO_4^{[-2]}$ and $>YOH_2CrO_4^{[-1]}$ were set to 8.7 and 9.4 for all calculations.

CHAPTER V

CONCLUSIONS

Experimental Conclusions

There are many parameters that influence adsorption of metals and metalloids on to soils, including pH, ionic strength, pCO_2, and the presence of competing ions. For anions such as Cr(VI), adsorption is typically greatest at lower pH, and decreases with increasing pH. This would have a significant influence on Cr(VI) adsorption in natural environments if a contaminated aquifer also had a very low pH.

Another important factor affecting Cr(VI) adsorption is the ionic strength of the solution. This affects adsorption by influencing the net charge of the mineral surfaces, and the extent of the resulting electrical double layer (edl). The edl is compressed at higher solution ionic strengths and extends further into solution at lower ionic strengths. Cr(VI), an anion, sorbs onto HMO at pH conditions at which the mineral surface is negatively charged, presumably due to strong covalent/chemical interactions between manganese and chromium. Thus, at higher ionic strengths, when the edl is more compressed, increased adsorption is observed compared to lower ionic strengths, when the edl extends further into the solution.

Another potentially important influence on Cr(VI) adsorption is competition with other anions. In this study, competition with carbonate anions was investigated by conducting experiments under a variety of pCO_2 levels. Because aqueous carbonate may compete with chromate for surface sites, increasing the pCO_2 of the environment is expected to decrease chromate adsorption, due to the increased concentration of aqueous carbonate. However, even at high pCO_2 (5%), relatively little change in Cr(VI) adsorption was observed compared to low pCO_2 experiments. The observed dependence of Cr(VI) adsorption on carbonate level was not systematic: the atmospheric pCO_2 experiments generally exhibited the greatest adsorption, followed by 2.5% and 5% pCO_2 experiments, respectively, with 0% pCO_2

experiments displaying similar adsorption to that observed at 5% pCO_2 for two of the three ionic strengths investigated. This suggests that the error in measuring the edges may be greater than any influence of carbonate competition under the conditions considered in this study.

Model Conclusions

Reaction stoichiometries and equilibrium constants for formation of Cr(VI) surface complexes were derived using the DLM developed by Tonkin et al. (2004). The new reactions and equilibrium constants were added to the Tonkin thermodynamic database in Visual MINTEQ. The reaction stoichiometries and respective equilibrium constants derived for formation of Cr(VI) and carbonate surface complexes for the single chromate surface complex DLM are:

$$>XOH + CrO_4^{[-2]} = >XOHCrO_4^{[-2]} \qquad (8.57) \qquad (5.1)$$

$$>YOH + H^{[+1]} + CO_3^{[-2]} = >YOH_2CO_3^{[-1]} \qquad (17.17) \qquad (5.2)$$

This model predicts Cr(VI) adsorption on HMO reasonably well over a wide range of conditions including variations in pH, ionic strength, pCO_2, and differing sorbate to sorbent ratio. The model accurately describes adsorption under 0% pCO_2 conditions for ionic strengths spanning two orders of magnitude and pH ranges of ~3-10. Under 5% and 2.5% pCO_2 conditions, the model accurately describe adsorption at 0.01 M $NaNO_3$, but underestimates adsorption for 0.001 M $NaNO_3$ and overestimates adsorption for 0.1 M $NaNO_3$ experiments. Under 5% pCO_2 conditions, the model overestimates all experimental data without the addition of the carbonate surface complex and underestimates all ionic strength conditions with the addition of the carbonate surface complex. Under a different Cr(VI) loading ($2 \cdot 10^{-5}$ M Cr(VI) and 20 g/L HMO), the fits the experimental data collected at 5% pCO_2 and 0.01 M $NaNO_3$ fairly well, and underestimates adsorption compared to data collected at 5% pCO_2 and 0.001 M $NaNO_3$. Overall, the model adequately represents the experimental data without the addition of a carbonate surface complex for many conditions and has the

power to correctly describe Cr(VI) adsorption on HMO over a wide range of solution conditions.

The reaction stoichiometries and respective equilibrium constants derived for formation of Cr(VI) and carbonate surface complexes for the dual chromate surface complex DLM are:

$$>XOH + CrO_4^{[-2]} = >XOHCrO_4^{[-2]} \quad (8.7) \quad (5.3)$$

$$>YOH + H^{[+1]} + CrO_4^{[-2]} = >YOH_2CrO_4^{[-1]} \quad (9.4) \quad (5.4)$$

$$>XOH + CO_3^{[-2]} = >XOHCO_3^{[-2]} \quad (12.0) \quad (5.5)$$

This models predicts Cr(VI) adsorption on HMO reasonably well over a wide range of conditions including variations in pH, ionic strength, pCO_2, and differing sorbate to sorbent ratio. The models accurately describes adsorption under both 0% pCO_2 conditions and 5% pCO_2 conditions for ionic strengths spanning two orders of magnitude and pH ranges of ~3-10. Under 2.5% and atmospheric pCO_2 conditions, the models accurately describe adsorption at 0.01 M $NaNO_3$, but underestimates adsorption for 0.001 M $NaNO_3$ and overestimates adsorption for 0.1 M $NaNO_3$ experiments. Under a different Cr(VI) loading ($2 \cdot 10^{-5}$ M Cr(VI) and 20 g/L HMO), the model slightly overestimates data collected at 5% pCO_2 and 0.01 M $NaNO_3$, and underestimates adsorption compared to data collected at 5% pCO_2 and 0.001 M $NaNO_3$. Overall, the model adequately represents the experimental data and has the power to correctly describe Cr(VI) adsorption on HMO over a wide range of solution conditions. However, it does not significantly improve fits compared to the simpler model with only a single chromate surface complex.

Future Work

Despite the reasonably good fits the derived DLM parameters can provide for Cr(VI) adsorption on HMO, more work should be completed to continue to test and improve the robustness of this DLM. First, several of the experiments should be duplicated to check for reproducibility, notably experiments conducted with 0.001 and 0.01 M $NaNO_3$ at 0% pCO_2 and with 0.001 M $NaNO_3$ at 2.5% pCO_2 (all with

$1 \cdot 10^{-5}$ M Cr(VI) and 20 g/L HMO). Cr(VI) adsorption in these experiments was markedly lower than expected based on observed trends in pCO_2 dependence at single ionic strength conditions. Further experiments should also be conducted under various Cr(VI) loadings, and especially at pCO_2 conditions other than 5%, to test the ability of the model to accurately predict adsorption under different sorbate to sorbent ratios.

Carbonate was shown to affect higher pCO_2 conditions greater than lower pCO_2 conditions, and measuring the carbonate competing with chromate adsorption would improve model accurateness. Dissolved carbonate was calculated theoretically through measurements of pCO_2 and pH of the experimental solution in the thermodynamic database Visual MINTEQ. Thus any experimental errors incurred by measuring both the pCO_2 and pH in the experiments used to optimize the carbonate surface complex, are systematically incurred for all conditions where carbonate exists in the model. Direct measurement of sorbed carbonate for each experiment is preferred, but beyond the scope of this study and because of specialized equipment required.

To ensure the accuracy of the DLM, more information regarding bond interactions and surface sites are desired. Quantum mechanics can be used to deduce more energetically favorable bond interactions that would exist in the system, however this requires specialized expertise, and is currently beyond the scope of this study. Spectroscopic information, such as extended X-ray absorption fine structure (EXAFS) spectroscopy can also yield detailed information regarding mineral surfaces including bond interactions as well as coordination numbers and composition of neighbor atoms of the mineral. EXAFS require access to synchrotron beam such as can be found at the national laboratory in Argonne Illinois.

Appendix A

Adsorption Edge Kinetics

Experiment B: Atmospheric pCO_2, 0.001 M $NaNO_3$,

$1 \cdot 10^{-5}$ M Cr(VI) and 20 g/L HMO

pH	% Adsorbed
2.93	83.70
3.57	73.35
4.28	62.38
4.83	54.23
5.41	40.13
6.19	16.30
6.74	13.48
7.67	0.31
8.62	1.57
9.24	-2.19

Experiment C: Atmospheric pCO_2, 0.01 M $NaNO_3$,

$1 \cdot 10^{-5}$ M Cr(VI) and 20 g/L HMO

pH	% Adsorbed
3.09	88.13
3.77	81.25
4.39	74.69
5.25	62.50
5.73	51.88
6.28	29.69
6.75	13.13
7.58	0.00
8.42	0.00
9.2	0.00

Experiment D: Atmospheric pCO_2 and 0.1 M $NaNO_3$,

$1 \cdot 10^{-5}$ M Cr(VI) and 20 g/L HMO

pH	% Adsorbed
3.02	94.62
3.63	93.35
4.23	83.54
4.82	87.34
5.25	84.81
5.75	74.68
6.3	44.30
7.06	9.81
8.01	4.11
9.27	0.00

Experiment F: 2.5% pCO_2 and 0.001 M $NaNO_3$,

$1 \cdot 10^{-5}$ M Cr(VI) and 20 g/L HMO

pH	% Adsorbed
3.08	72.70
3.29	66.98
3.86	55.24
4.34	47.62
4.99	34.29
5.55	24.76
5.95	12.06
6.7	18.73
6.72	8.57
7.31	0.00

Experiment G: 2.5% pCO_2, 0.01 M $NaNO_3$,

$1 \cdot 10^{-5}$ M Cr(VI) and 20 g/L HMO

pH	% Adsorbed
3.12	82.22
3.33	80.00
4.44	68.25
5.2	57.46
5.71	45.40
6.11	31.11
6.45	25.71
6.8	22.22
7.32	17.78
8.42	12.70

Experiment H: 2.5% pCO_2, 0.1 M $NaNO_3$,

$1 \cdot 10^{-5}$ M Cr(VI) and 20 g/L HMO

pH	% Adsorbed
3.01	94.64
3.51	92.86
4.1	90.18
4.78	83.63
5.39	71.73
6.02	45.54
6.62	19.35
7.16	4.17
7.84	0.00
9.02	0.00

Experiment J: 5% pCO_2, 0.001 M $NaNO_3$,

$1 \cdot 10^{-5}$ M Cr(VI) and 20 g/L HMO

pH	% Adsorbed
2.87	54.96
3.54	36.52
4.43	23.76
5.31	10.99
5.94	2.84
6.62	0.00
7.32	0.00
7.95	0.00
8.75	2.13
9.21	0.00

Experiment K: 5% pCO_2, 0.01 M $NaNO_3$,

$1 \cdot 10^{-5}$ M Cr(VI) and 20 g/L HMO

pH	% Adsorbed
2.51	82.49
3.15	87.44
3.9	65.99
4.58	54.55
5.22	40.74
5.66	28.28
6.58	8.42
7.25	2.69
7.96	0.00
8.99	0.00

Experiment L: 5% pCO_2, 0.1 M $NaNO_3$,

$1 \cdot 10^{-5}$ M Cr(VI) and 20 g/L HMO

pH	% Adsorbed
2.99	94.57
3.57	92.29
4.23	88.57
4.93	80.57
5.57	67.14
6.05	49.14
7.07	9.71
7.52	3.71
8.68	-1.43
9.42	-0.57

Experiment N: 0% pCO_2, 0.001 M $NaNO_3$,

$1 \cdot 10^{-5}$ M Cr(VI) and 20 g/L HMO

pH	% Adsorbed
3.16	52.63
3.72	40.79
4.31	37.83
4.88	17.76
5.79	10.86
6.53	1.64
7.36	0.00
8.16	2.30
9.16	0.00
10.22	0.00

Experiment O: 0% pCO_2, 0.01 M $NaNO_3$,

$1 \cdot 10^{-5}$ M Cr(VI) and 20 g/L HMO

pH	% Adsorbed
3.21	75.37
3.8	67.54
4.4	60.45
4.99	50.75
5.57	33.96
6.34	12.69
6.7	19.03
7.41	-2.61
8.47	-2.99
9.16	-9.33

Experiment P: 0% pCO_2, 0.1 M $NaNO_3$,

$1 \cdot 10^{-5}$ M Cr(VI) and 20 g/L HMO

pH	% Adsorbed
2.98	95.77
3.62	94.56
4.2	92.45
4.91	90.03
5.5	85.20
6.01	76.13
6.79	34.44
7.48	10.57
8.6	5.44
9.83	4.53

Experiment Q: 0% pCO_2, 0.001 M $NaNO_3$,

$2 \cdot 10^{-5}$ M Cr(VI) and 20 g/L HMO

pH	% Adsorbed
2.59	81.21
3.59	66.06
4.34	54.55
5.17	37.58
5.81	26.67
6.01	23.64
6.56	10.91
7.02	15.15
8.32	5.45
8.85	0.00

Experiment R: 0% pCO_2, 0.1 M $NaNO_3$,

$2 \cdot 10^{-5}$ M Cr(VI) and 20 g/L HMO

pH	% Adsorbed
2.81	84.57
4.47	79.43
4.13	72.00
4.76	59.43
5.6	39.43
6.12	7.43
6.48	8.57
8.89	9.71
9.58	9.71
9.46	7.43

Appendix B

Kinetic Experiments

Kinetic experiment: Atmospheric pCO_2, 0.001 M $NaNO_3$,

$1 \cdot 10^{-5}$ M Cr(VI) and 5 g/L HMO; starting pH 3 then raised to pH 10 at 18.48 hours

Time (hrs)	% Adsorbed
0.00	10.61
0.08	29.39
0.17	32.73
0.25	37.58
0.33	40.00
0.53	42.73
0.75	49.70
1.00	51.52
1.57	52.73
18.10	57.58
18.48	3.33
18.58	1.82
18.67	1.82
18.92	0.30
19.42	0.00

Kinetic experiment: Atmospheric pCO_2, 0.001 M $NaNO_3$,

$1 \cdot 10^{-5}$ M Cr(VI) and 10 g/L HMO; starting pH 3 then raised to pH 10 at 44.55 hours

Time (hrs)	% Adsorbed
0.00	14.46
0.08	29.22
0.25	37.95
0.50	44.58
0.83	53.01
2.33	57.53
2.83	57.83
3.25	58.13
21.33	60.84
22.42	56.02
24.17	61.45
26.92	65.66
43.95	66.57
44.38	66.87
44.55	7.23
44.88	7.83
45.33	2.11

Timed adsorption edge experiment: 4, 24, and 48 hours equilibration time,

Atmospheric pCO_2, 0.001 M $NaNO_3$,

$1 \cdot 10^{-5}$ M Cr(VI) and 10 g/L HMO

4 hours equilibration time		24 hours equilibration time		48 hours equilibration time	
pH	% Adsorbed	pH	% Adsorbed	pH	% Adsorbed
3.12	46.97	3.02	53.80	3.3	47.43
3.45	41.50	3.3	42.98	3.64	46.00
4.1	33.43	3.95	33.04	4.32	36.57
4.5	27.38	4.35	26.02	4.7	28.57
5.05	20.17	4.92	20.47	5.28	24.00
5.56	12.68	5.62	11.99	5.89	18.00
5.91	11.82	5.83	9.36	6.23	14.86
6.5	10.09	6.33	8.19	6.8	12.86
7.2	9.51	7.06	6.43	7.55	10.00
8.1	10.37	7.85	5.26	8.25	14.00
9.23	10.37	9.05	7.02	9.14	11.43

Timed adsorption edge experiment: 24, 48, and 72 hours equilibration time,

Atmospheric pCO_2, 0.01 M $NaNO_3$,

$1 \cdot 10^{-5}$ M Cr(VI) and 20 g/L HMO

24 hours equilibration time		48 hours equilibration time		72 hours equilibration time	
pH	% Adsorbed	pH	% Adsorbed	pH	% Adsorbed
3.13	88.57	3.19	88.06	3.13	86.39
3.67	82.54	3.73	79.03	3.58	81.01
4.21	76.19	4.24	75.16	4.15	75.63
4.83	66.35	4.88	65.81	4.8	66.46
5.25	55.56	5.3	55.48	5.24	55.70
5.62	46.98	5.67	43.23	5.63	45.25
6.21	16.83	6.2	19.03	6.18	25.32
6.93	9.52	6.91	5.81	6.94	12.03
8.17	2.54	8.19	0.303	8.04	0.299
9.43	4.13	9.32	0.298	9.19	0.281

BIBLIOGRAPHY

Agency for Toxic Substances and Disease Registry (ATSDR), (2012). *Toxicological profile for chromium*. Retrieved from website: http://www.atsdr.cdc.gov/toxprofiles/tp7.pdf

Allison, J.D., Brown, D.S., Novo-Gradac, K.J., 1991. MIN- TEQA2/PRODEFA2, A geochemical assessment model for environmental systems: Version 3.0 User's Manual. U.S. Environmental Protection Agency, Athens, GA.

Balistrieri, L.S., Murray, J.W., 1982. The surface chemistry of dMnO2 in major ion seawater. Geochim. Cosmochim. Acta 46, 1041–1052.

Balistrieri, L. S., Murray, J. W., & Paul, B. (1992b). The biogeochemical cycling of trace metals in water column of lake sammamish, washington: Response to seasonally anoxic conditions. *Limnology and Oceanography*, *37*(3), 529-548.

Barnhart, J. (1997). Occurrences, uses, and properties of chromium. *Regulatory Toxicology and Pharmacology*, *26*, S3-S7.

Borch, T., Kretzschmar, R., Kappler, A., Van Cappellen, P., Ginder-Vogel, M., Voegelin, A., Campbell, K. (2010). Biogeochemical redox process and their impact on contaminant dynamics. *Environmental Science and Technology*, (44), 15-23.

Catts, J.G., Langmuir, D., 1986. Adsorption of Cu, Pb and Zn by dMnO2: applicability of the site binding-surface com- plexation model. Appl. Geochem. 1, 255–264.

Cohen, M. D., Kargacin, B., Klein, C. B., & Costa, M. (1993). Mechanisms of chromium carcinogenicity and toxicity. *Critical Reviews in Toxicology*, *23*(3), 255-281.

Costa, M. (1997). Toxicity and carcinogenicity of cr(vi) in animal models and humans. *Critical Reviews in Toxicology*, *27*(5), 431-442.

Costa, M., & Klein, C. B. (2006). Toxicity and carcinogenicity of chromium compounds in humans. *Critical Reviews in Toxicology*, (36), 155-163.

Dai, R., Liu, J., Yu, C., Sun, R., Lan, Y., Mao, J.D. (2009). A comparative study of oxidation of cr(iii) in aqueous ions, complex ions and insoluble compounds by manganese-bearing mineral (birnessite). *Chemosphere*, (76), 536-541.

Daneshvar, N., Salari, D., and Aber, S. (2002). Chromium adsorption and cr(vi) reduction to trivalent chromium in aqueous solutions by soya cake. *Journal of Hazardous Materials*, (B94), 49-61.

Davis, J.A., Kent, D.B., 1990. Surface complexation modeling in aqueous geochemistry. In: Hochella, M.F., White, A.F. (Eds.), Reviews in Mineralogy. Mineralogical Society of America, Washington, D.C, pp. 177–260.

Davison, W., 1993. Iron and Manganese in Lakes. *Earth-Science Reviews*, 34, 119-164.

Drits, V.A., Silvester, E., Gorshkov, A.I., Manceau, A., 1997. Structure of synthetic monoclinic Na-rich birnessite and hexagonal birnessite: I. Results from X-ray diffraction and selected-area electron diffraction. Am. Mineral. 82, 946–961.

Dzombak, D.A., Morel, F., 1990. Surface Complexation Modeling : Hydrous Ferric Oxide. Wiley, New York.

Eary, L. E., & Ral, D. (1987). Kinetics of chromium(iii) oxidation to chromium(v1) by reaction with manganese dioxide. *Environmental Science and Technology*, (21), 1187-1193.

Eby, G. (2004). *Principles of environmental geochemistry*. Belmont, Ca: Brooks/Cole.

Fendorf, S., & Zasoski, R. J. (1992). Chromium(III) oxidation by δ-MnO_2. 1. characterization . *Environmental Science and Technology*, (26), 79-85.

Fu, G., Allen, H.E., Cowan, C.E., 1991. Adsorption of cadmium and copper by manganese oxide. Soil Science 152, 72–81.

Giovanoli, R., Stahli, E., Feitknecht, W., 1970a. Über oxidhydroxide des vierwertigen mangans mit schichtengitter. 1. Natriummangan(II,III)manganat(IV). Helv. Chim. Acta 53, 209–220.

Grevatt, P. C. U.S. Environmental Protection Agency, (1998). *Toxicological review of hexavalent chromium* (18540-29-9). Retrieved from website: http://www.epa.gov/iris/toxreviews/0144tr.pdf

Holmes, A. L., Wise, S. S., & Wise, J. P. (2008). Carcinogenicity of hexavalent chromium. *Indian Journal of Medical Research*, *128*(4), 353-372.

Huang, C. P., & Wu, M. H. (1975). Chromium removal by carbon adsorption. *Water Pollution Control Federation*, *47*(10), 2437-2446.

Jardine, P. M., Fendorf, S. E., Mayes, M. A., Larsen, I. L., Brooks, S. C., & Bailey, W. B. (1999). Fate and transport of hexavalent chromium in undisturbed heterogeneous soil. *Environmental Science and Technology*, (33), 2939-2944.

Koretsky, C. M. (2000). The significance of surface complexation reactions in hydrologic systems: a geochemist's perspective. *Journal of Hydrology*, (230), 127–171.

Mathur, S.M., 1995. Development of a Database for Ion Sorption on Goethite Using Surface Complexation Model- ing. M.S. thesis, Carnegie Mellon University.

McKenzie, R.M., 1981. The surface charge on manganese dioxides. Australian Journal of Soil Research 19, 41–50.

Nesse, W. D. (2000). *Introduction to mineralogy*. Oxford University Press, USA.

Patterson, R. R., & Fendorf, M. (1997). Reduction of hexavalent chromium by amorphous iron sulfide. *Environmental Science and Technology*, *31*, 2039-2044.

Paulson, A.J., 1996. Fate of metals in surface waters of the Coeur d'Alene Basin, Idaho. United States Department of the Interior Bureau of Mines Report of Investigations, Rept. 9620.

Post, J.E., 1999. Manganese oxide minerals: crystal structures and economic and environmental significance. Proceedings of the National Academy of Sciences, USA 96, 3447–3454.

Pretorius, P.J., Linder, P.W., 2001. The adsorption character- istics of d-manganese dioxide: a collection of diffuse double layer constants for the adsorption of H+, Cu2+, Ni2+, Zn2+, Cd2+ and Pb2+. Appl. Geochem. 16, 1067–1082.

Ran, Y., Fu, J., 1999. Adsorption of Au(III) and Au(I) com- plexes on d-MnO2. Sci. China (Series D) 42, 172–181.

U.S. Environmental Protection Agency, (1999). *The class v underground injection control study; volume 1 study approach and general findings; appendix e* (816-R-99-014a). Retrieved from website: http://water.epa.gov/type/groundwater/uic/class5/upload/2007_12_12_uic_class5_study_uic-class5_classvstudy_persist_appe.pdf

Tokunaga, T. K., Wan, J., Lanzirotti, A., Sutton, S. R., Newville, M., & Rao, W. B. (2007). Long-term stability of organic carbon-stimulated chromate reduction in contaminated soils and its relation to manganese redox status. *Environmental Science and Technology*, (41), 4326-4331.

Tonkin, J. W., Balistrieri, L. S., & Murray, J. W. (2004). Modeling sorption of divalent metal cations on hydrous manganese oxide using the diffuse double layer model. *Applied Geochemistry*, (19), 29–53.

Westall, J., Hohl, H., 1980. Comparison of electrostatic models for the oxide-solution interface. Adv. Coll. Interface Sci. 12, 265–294.

WHO, (1996). *Chromium in drinking water; background document for development of who guidelines for drinking-water quality* (2nd Edition, Vol. 2). Retrieved from World Health Organization website: http://www.who.int/water_sanitation_health/dwq/chemicals/chromium.pdf